Alteration of microstructure in biopolymeric hydrogels via compositional modification of resilin-like polypeptides

Cristobal Garcia Garcia[a], Sai S. Patkar[a], Nina Jovic[b], Jeetain Mittal[b], Kristi L. Kiick[a,c,d,]*

[a] Department of Materials Science and Engineering, University of Delaware, Newark, DE 19716, USA

[b] Department of Chemical and Biomolecular Engineering, Lehigh University, Bethlehem, PA 18015, USA

[c] Delaware Biotechnology Institute, Newark, DE 19716, USA

[d] Biomedical Engineering, University of Delaware, Newark, DE 19176, USA

Keywords: Resilin, UCST, phase-separation, hydrogel,

Abstract

Heterogeneities in hydrogel scaffolds are known to impact the performance of cells in cell-laden materials constructs, and we have employed the phase separation of resilin-like polypeptides (RLPs) as a means to generate such materials. Here, we study the compositional features of resilin-like polypeptides (RLPs) that further enable our control of their liquid-liquid phase separation

(LLPS), and how such control impacts the formation of microstructured hydrogels. Evaluation of phase separation of RLPs in solutions of ammonium sulfate offers insights into the sequence-dependent LLPS of the RLP solutions, and atomistic simulations, along with 2D NOESY and COSY ^{1}H NMR, suggest specific amino acid interactions that may mediate this phase behavior. Acrylamide functionalization of RLPs enables their photo-crosslinking into hydrogels and also enhances the phase separation of the polypeptides. A heating-cooling protocol promotes the formation of stable emulsions that yield different microstructured morphologies with tunable rheological properties. These findings offer approaches for choosing RLP compositions with phase behavior that can be easily tuned with differences in temperature and time, to control the resulting morphology and mechanical behavior of the heterogeneous hydrogels in regimes useful for biological applications.

1. Introduction

Since the establishment of the central dogma of structural biology,[1] an enormous body of work has confirmed the key role of three-dimensional protein structure on protein function. It has only been in the past few decades that the *in vivo* functions mediated by intrinsically disordered proteins (IDPs), which lack such three-dimensional structure, has been appreciated.[2–5] IDPs have a critical cytoplasmic role in forming membraneless organelles such as nucleoli, Cajal bodies, stress-granules, and P-bodies, among others, [6–8] enabled by their liquid-liquid phase separation (LLPS),[9–11] which can be regulated by local environmental changes such as pH, ion concentrations, and/or binding of ligands.[12–15] This LLPS-mediated concentration of molecules mediates the function attributed to the organelle itself. [16–18]

LLPS of IDPs has also been leveraged in materials science applications for many decades, for a variety of purposes such as hydrogel formation,[19,20] cargo recruitment and delivery,[17,21] and

assembly of artificial membraneless organelles.[22,23] Most of this work has been established with elastin-like polypeptides (ELPs), although more recently the use of resilin-like polypeptides (RLPs) has emerged. ELPs are among the most studied resources for these applications due to their easily accessible and tunable lower critical solution temperature (LCST).[24,25] Control of ELP phase separation by manipulation of temperature, composition, and time has facilitated the production of scaffolds with unique architectures such as bead-string microstructures[24] and multilayered cylinders,[26] and special features such as self-healing, high elasticity, and self-adhesion can be incorporated by manipulation of the peptide sequence.[26,27] Other IDPs that have been used in materials applications exploit different structural properties. For instance, repeat-in-toxin (RTX) elastomeric proteins have the ability to change from a disordered to an ordered (β-roll) conformation upon addition of Ca^{2+}, and have found application in shrinkable/swellable hydrogels.[28,29] Phenylalanine-glycine-rich nucleoporins are IDPs involved in the permeability barrier of nuclear transport. The phenylalanine content of their sequence has been shown to control the crosslinking of pH-sensitive hydrogels for in vitro models of nuclear transport systems.[30] RLPs have also found applications in materials due to their outstanding mechanical properties and upper critical solution temperature (UCST).[31–33] Chemical modifications and temporal control over the phase separation of RLPs have been used to tune the final characteristics of hydrogels; microstructure size and micromechanical properties, for instance, with an impact in cell-guided proliferation.[34,35]

Resilin is an elastomeric, insect-derived IDP, which exhibits exceptional resilience with potential value in the regeneration of mechanically active tissues (e.g., vocal folds[31,36,37] or cardiovascular tissue[38,39]). Among the variables that can promote the LLPs of IDPs, temperature, concentration, molecular weight, pH, ion type and incorporation of molecular crowding agents

such as poly(ethylene glycol) (PEG) are the most common.[12,40–43] For intrinsically disordered proteins and polypeptides, control of amino acid composition also provides a sensitive variable for modulating LLPS, which has been used to great effect in the engineering of myriad types of ELPs. The UCST-like LLPS in IDPs is driven by interactions between polar, ionic, and aromatic residues by means of charge-charge, cation-π, dipole-dipole, π-π stacking, and π-sp^2 interactions.[12,44–46] More specifically, literature reports evidence of interactions between positively charged amino acids as arginine and lysine and aromatic amino acids as tryptophan, tyrosine and phenylalanine.[47–49] In contrast, the LCST-like phase separation of IDPs is driven by loss of hydration and a subsequent increase of hydrophobic interactions between non-polar residues.[50–52]

Early work on RLPs illustrates that the native sequence derived from the first exon of *Drosophila melanogaster* CG15920 gene, which comprises 18 repeats of the amino acid repeat GGRPSDSYGAPGGGN, has both UCST and LCST.[53–55] It has been shown that the former transition is due to the polar and aromatic interactions of the GGRPSDSY sequence,[12,44] while the latter is due to hydrophobic interactions of the GAPGGGN sequence, as in the case of ELPs.[50,56] To date, RLPs are the only IDP reported with dual-phase behavior.[57] RLP sequences developed previously in our laboratories are based on the native resilin sequence of *Drosophila melanogaster*, with differences including that 12 repeats of the putative sequence are employed instead of 18 and the central tyrosine on each repeat has been substituted with phenylalanine or methionine. This change in the natural sequence resulted in a lack of a UCST transition, and LCST behavior was the only LLPS observed in these sequences.[41] In this work, new RLP sequences were produced with substitutions in the central amino acid in the RLP domain to different aromatic (tryptophan, tyrosine, phenylalanine) and aliphatic (leucine, valine, alanine) residues. These substitutions enable the investigation of the impact of these key amino acids on the UCST transition, with an

aim to use sequence to control microstructures in cytocompatible hydrogels. Turbidity measurements were performed to determine the effect of the amino acid substitutions and acrylamide functionalization on the transition temperatures of the RLP. All-atom computer simulations and 2D ^{1}H NMR experiments were conducted to identify amino acid residues likely to mediate the phase transition. Polypeptides with favorable transition temperatures were used to fabricate microstructured hydrogels via a heating-cooling induction of phase separation, followed by photo-crosslinking of the emulsion. Confocal microscopy was employed to characterize the microstructures, and oscillatory rheology studies were performed to evaluate the bulk mechanical properties of the microstructured materials, which were shown to be correlated with the hydrogel microstructure.

2. Material and methods

2.1. Materials

The plasmid DNA encoding the different RLP sequences in pQE80 was purchased from Genscript Corporation (Piscataway, NJ). Chemically competent cells of E. coli strain M15-[pREP4] (for transformation of recombinant plasmids) and RNAse (for protein purification) were purchased from Qiagen (Valencia, CA). Deuterium oxide and NMR solvents were purchased from Cambridge Isotope Laboratories (Tewksbury, MA). All other chemicals were obtained from Sigma-Aldrich (St. Louis, MO) or Fisher Scientific (Waltham, MA) and were used as received unless otherwise noted.

2.2. Protein Expression and Purification

Each DNA plasmid was transformed into the E. coli M15 [pREP4] strain by heat shock to generate the expression cell stocks employed in protein production. RLP-X (based on the repeat GGRPSDSXGAPGGGN, see Figure S1 for the detailed sequence) protein expression and

purification were conducted as previously reported by our laboratories.[36,58–60] In brief, a single colony of *E. coli* M15[pREP4] containing the desired RLP construct was inoculated in 150 mL of sterile LB media containing 100 μg mL^{-1} antibiotics (ampicillin) and grown overnight. Overnight culture media (150 mL) was used to evenly inoculate 6x750 mL of 2xTY media (yeast 10 g L^{-1}, NaCl 5 g L^{-1}, and tryptone 16 g L^{-1}) for protein expression. The 750 mL cultures were grown in a shaker at 37°C until the OD600 reached 0.6−0.8, and then isopropyl β-D-1-thiogalactopyranoside (IPTG) was added to a final concentration of 1 mM to induce protein expression. After 4 h of culture for protein expression, cells were harvested by centrifugation (5000 rpm for 15 min at 4°C), and cell pellets were stored at −20 °C. The frozen cell pellets were lysed by freeze−thaw cycles, and the lysed cell pellets were suspended in pH 8.0 native lysis buffer (50 mM NaH_2PO_4, 300 mM NaCl, and 10 mM imidazole) with 0.45 g of lysozyme. Lysed cells were further disrupted via sonication on ice, using a Fisher Scientific model 500 Sonic Dismembrator (10 mm tapered horn) for 20 min with a 10-s recovery time and subsequently incubated with RNAse (10 μg mL^{-1}) and DNAse (5 μg mL^{-1}) for 30 minutes. The supernatant from centrifugation (20,000 rpm for 15 min at 4°C) of cell lysate was collected and heated to 80 °C for 5 min to remove hydrophobic proteins by centrifugation (4000 rpm for 60 min at 4°C). The supernatant was filtered, and pH was adjusted to 8.0, followed by incubation with Ni-NTA resin overnight at 4°C. The protein-loaded resin was then loaded into a gravitational flow column, washed with native lysis buffer, native wash buffer (50 mM NaH_2PO_4, 300 mM NaCl, and 20 mM imidazole, pH 8.0), and finally eluted with native elution buffer (50 mM NaH_2PO_4, 300 mM NaCl, and 250 mM imidazole, pH 8.0). 75 mL elution fractions were carefully transferred and dialyzed (MWCO 10 kDa) against deionized water (5 L) at 4 °C with at least 6 changes of water before sterile filtration and lyophilization. The protein yield was approximately 30−50 mg per liter of cell culture.

2.3. Acrylamide Functionalization and Characterization

The RLP proteins were functionalized with acrylamide groups via modification of regularly positioned lysine residues of the polypeptide chain. First, the RLP proteins were dissolved in PBS (5 mg mL^{-1}). NHS-activated acrylic acid (NHS-Ac) was dissolved in dimethyl sulfoxide (DMSO) in 50 mg mL^{-1} separately and drop-wise added into the RLP solution. The ratio of NHS-Ac to lysine was varied depending upon the desired functionality of the conjugate. The reaction was stirred at room temperature for ≈4 h. This reaction solution was diluted eight times with DI water to prevent precipitation and dialyzed (Snakeskin, 3.5 kDa, Thermo Scientific) against DI water at 4 °C (in a cold room) to remove byproducts and DMSO. The purified RLP-X-Ac was filtered and lyophilized and stored at −20 °C prior to experiment. The functionality of the RLP-X-Ac was characterized via 1H NMR spectrometry. The purified RLP-X-Ac (≈2 mg) was dissolved in (600 µl) D2O (Cambridge Isotope Laboratories, Tewksbury, MA) and analyzed using an AVIII 600 MHz NMR spectrometer (Bruker Daltonics, Billerica, MA). The protons from the thirteen aromatic residues per RLP molecule were used as an internal reference for the quantification of acrylamide group functionality. The integration of the aromatic protons of phenylalanine (^{1}H NMR (600 MHz, D2O, δ): 7.15–7.40 (m, 5H)) tyrosine (^{1}H NMR (600 MHz, D2O, δ): 6.67 (m, 2H), 6.98 (m, 2H)), or tryptophan (^{1}H NMR (600 MHz, D2O, δ): 7.00–7.60 (m, 5H)) was compared to the integration of the vinylic protons of the acrylamide that resulted from the reaction of the acrylamide and lysine amine groups (^{1}H NMR (600 MHz, D2O, δ): 5.65–6.30 (d, 3H)).

2.4. General Characterization of RLPs

Amino acid analysis was performed by the Molecular Structure Facility at the University of California, Davis (Davis, CA) using a Hitachi L-800 sodium citrate-based amino acid analyzer (Tokyo, Japan) to determine the composition of each RLP polypeptide. The purity and molecular

weight of the peptides was confirmed via UPLC and electrospray ionization mass spectrometry (ESI-MS) (Waters Xevo G2-S Q-TOF MS with Acquity UPLC, Milford, MA), and corroborated *via* matrix-assisted laser desorption/ionization-time of flight mass spectrometry (Bruker MicroFlex MALDI-TOF, Billerica, MA). Samples that showed a small degree of impurities were purified via reverse-phase HPLC (Waters Inc., Milford, MA) on a Waters Xbridge BEH130 Prep C-18 column. The mobile phase comprised gradients of degassed deionized water with 0.1% TFA and acetonitrile with 0.1% TFA, at a flow rate of 30 mL min^{-1}. The peptide was detected by UV detectors at 214 nm and 280 nm; fractions with product were collected and lyophilized and confirmed again by ESI-MS. FTIR spectroscopy experiments were performed using a Nexus 670 FTIR spectrometer (Thermo Nicolet, Madison, Wisconsin) with unpolarized light and an MCT detector to determine the conformational changes on the different sequences. The PIKE MIRacle™ single reflection ATR with high IR throughput was used as a universal ATR sampling accessory for analysis of RLP-X solution. 10μL of 80 mg/mL RLP solution in D_2O was dropped on the diamond crystal plate to ensure good contact before collecting the spectra. Spectra were recorded from 400 to 4000cm^{-1} at a resolution of 4 cm^{-1}. Each measurement was obtained by signal averaging 32 scans and three such measurements were made per droplet. The raw data was deconvoluted (Gaussian peaks) using the multiple-peak fitting function in Origin Data Analysis software (OriginLab, Northampton, MA) into peaks corresponding Amide II (1585 cm^{-1}), and Amide I (1600 to 1700 cm-1; β sheet (1622 cm^{-1}), Random coil (1645 cm^{-1}), β turn (1674 cm^{-1})).

2.5. RLP-X Phase Separation

RLP-X or RLP-X-Ac were dissolved in DI water at various concentrations in order to get an 8 mg mL^{-1} final concentration and the desired salt concentration when mixed with 2M stock solutions of NaCl, NH_4Cl, Na_2SO_4, or $(NH_4)_2SO_4$ in DI water. The phase diagrams were

determined by measurement of the turbidity of the RLP solutions under various solution conditions, via UV–Vis spectroscopy with a 10 mm path length quartz cuvette at a wavelength of 600 nm. The measurements were performed by cooling a series of RLP-X or RLP-X-Ac solutions from 85°C to 5°C at a rate of 1°C min^{-1}. The transition point was identified as the inflection point of transmittance increase from a Boltzmann fitting. UV–Vis spectroscopy was also used to obtain the temperature vs. composition phase diagram of RLP-W-4Ac in PBS (pH 7.4) by sequentially diluting 20 wt% solutions to 0.8 wt%.

2.6. Equilibrium Concentrations and NMR Spectroscopy

RLP-W-4Ac was dissolved in d-PBS at concentrations of either 5 wt% or 10 wt% and allowed to phase separate overnight into two immiscible layers either at room temperature (10 wt%, in order to corroborate phase separation data obtained via UV-Vis spectroscopy) or 4°C (5 and 10wt%, in order to expand the coexistence curve to lower and higher concentrations than those measured via turbidimetry). Samples were carefully collected from the top and from the bottom layer to prevent mixing of the two liquids and were dissolved in deuterium oxide (D_2O) that contained 0.01 mg mL^{-1} 4,4-dimethyl-4-silapentane-1-sulfonic acid (DSS) as an internal reference. The concentration of each component was calculated from the ^1H NMR spectrum acquired (128 scans) with a Bruker AVIII 600 MHz NMR spectrometer (Bruker Daltonics, Billerica, MA) under standard quantitative conditions. Standard DQF-COSY and NOESY ^1H NMR experiments were performed in the same instrument. The RLP-X samples and their acrylamide-functionalized analogs were dissolved in D_2O at 5 mg mL^{-1} to obtain a fully-soluble sample, and at 100 mg mL^{-1} to yield a phase-separated sample. The latter were prepared in special 5mm tubes with 3mm OD stem positioned in the sample holder at a height where the condensed phase (bottom phase) was aligned with the focus of the magnetic field.

2.7. Hydrogel Formation

The RLP-X-Ac was dissolved into PBS at a 10, 15, 20 wt% concentration. A stock solution of the photo-initiator lithium phenyl-2,4,6-trimethylbenzoylphosphinate (LAP) was prepared in PBS at a concentration of 13.4 mg mL^{-1}. A 5% volume of LAP solution was added to the RLP-X-Ac solution and vortex mixed the samples to obtain a final concentration of LAP of 2.2×10^{-3} M in the precursor mixture. The solution was warmed up in an Eppendorf 5333 MasterCycler Thermal Cycler to either 60°C or 80°C for 45s, cooled down in an ice bath for 30s, and transferred to a pre-cooled silicon chamber (5mm diameter, 0.5 mm thickness) and covered with a coverslip, a process which requires 30 to 40 seconds prior to initiating UV crosslinking. The sample was irradiated with UV light (365 nm, ≈5 mW cm^{-2}) for 4 min with a UVP Blak-Ray B-100AP high intensity UV lamp (UVP, Upland, CA). The UV intensity was confirmed with a radiometer. The cooling profiles for the two different initial temperatures were determined by warming up DI water, PBS, and RLP-W-4Ac 20wt% in PBS to 60°C or 80°C and cooled down in an ice bath. The temperature changes were registered every 10 seconds using a thermocouple system Fisherbrand Traceable Hi-Accuracy Thermometer (Fisher Scientific, Hampton, NH), and the generated cooling profiles were used to determine the final temperature of the precursor solutions after 30s in the ice bath. The microstructure was characterized with a Zeiss 780 multiphoton microscope (Carl Zeiss, Inc., Thornwood, NY), exploiting the autofluorescence of the RLP in the hydrogel. A Chameleon Vision II Multiphoton laser with a 755 nm wavelength was used to excite the autofluorescence of the RLP, and the NDD detection system was used for imaging the multiphoton fluorescence. The microstructure area analysis was performed in ImageJ setting the threshold of the image from50 to 255 in the gray scale to quantify the pixels corresponding to the RLP signal. The total area was referenced to the signal of a continuous RLP-F-4Ac 20wt% hydrogel.

2.8. Oscillatory Rheology

The oscillatory rheology experiments were conducted on an AR-G2 rheometer (TA Instruments, New Castle, DE) with an attached UV Light Guide accessory and UV lamp source (OmniCure S2000 (Excelitas)), with an 8 mm diameter stainless steel parallel-plate geometry. The precursor solutions were prepared *via* the warming-cooling protocol described above. The 10 µL hydrogel precursor solution was deposited on the quartz rheometer stage and the geometry was set at a 200 µm gap. Mineral oil was used to seal the geometry and prevented dehydration of the hydrogel. 365 nm UV with 5 mW cm^{-2} intensity was applied to induce UV crosslinking. The time that elapses prior to the start of UV crosslinking is 30 to 40 seconds, consistent with the time required to prepare microscopy samples. The mechanical properties of the hydrogels were measured in the linear viscoelastic regime where the modulus is independent of the level of applied stress or strain. The gelation of hydrogels was monitored using a time sweep conducted in the linear viscoelastic regime at 1% strain and an angular frequency of 6 rad s^{-1}, followed by a frequency sweep from 0.1 to 100 rad s^{-1} conducted at 1% strain and amplitude sweep from 0.1% to 1000% strain. Experiments were repeated on three samples for each condition and the shear modulus reported as the simple mean. The error is reported as the standard error of the samples tested.

2.9. Simulation Details

All atom single chain simulations were conducted using the Amber99SBws-STQ force field in the GROMACS[61] software package. Simulations were conducted using parallel tempering in the well-tempered ensemble (PT-WTE)[62] with 16 replicas at a range of temperatures of 300-518.4K. Initial configurations were generated by conducting 5 ns serial simulations at each temperature used in the parallel tempering and the production simulations were done for ~200ns. Simulations were analyzed at 300K. VDW contacts are defined as two groups having at least one heavy atom from

each group within 6 Å of each other. Hydrogen bonds are considered using the donor acceptor convention implemented in MDAnalysis, with a 3 Å distance and 120 degree angle cutoff. π-π contacts are defined as the COM of mass distance between the side chain atoms of the aromatic rings of Tyr, Trp and Phe with a 6 Å distance cutoff. Cation-π interactions are defined as the distance between the Guanidinium group of Arg/NH^{4+} group of Lys with the COM of the side chain atoms of the aromatic rings of Tyr, Trp and Phe with a 6 Å distance cutoff.

3. Results and Discussion

3.1. Polypeptide Design

The RLP sequence utilized in these studies is a 24 kDa polypeptide with 12 repeats of the amino acid sequence (GGRPSDSF/MGAPGGGN) based on the putative consensus sequence (GGRPSDSYGAPGGGN) of *Drosophila melanogaster*, five repeats of lysine-rich domains (GGKGGKGGKGG) useful for RLP functionalization purposes, an MMP-sensitive domain (GPQGIWGQG) derived from α(I) collagen relevant for cell remodeling in hydrogels, and an integrin-binding domain (GRGDSPG), derived from fibronectin, for promoting cell adhesion to the polymeric biomaterial.[58] This polypeptide was designated as RLP-F/M (where F/M indicates that phenylalanine and methionine are alternated over the 12 repeats). In contrast to the RLP sequence designed by Dutta, which preserves the putative Y-containing consensus sequence from *Drosophila melanogaster* with 18 repeats and showed a characteristic UCST-like transition,[55] the RLP-F/M lacked such a transition,[41] probably due to the substitution of the native tyrosine (Y) with phenylalanine (F) and methionine (M) in the consensus repeat. Supported by research claiming that cation-π and π-π stacking interactions are important for driving phase separation,[12,44–46] this evidence suggests that not only the inclusion of an aromatic amino acid is key to triggering the UCST-like transition, but also the identity of such residue has an impact and can be used to

tune the transition temperatures of the RLPs. Computational studies show that a key residue is arginine, being able to donate hydrogen bonds in addition to interacting with aromatic side chains.[47,63] Of the aromatic amino acids, tyrosine exhibits more contacts with arginine than phenylalanine due to the hydroxyl group that enhances the interaction, although tryptophan is the residue most often found in cation-π interactions compared with the other two aromatic residues.[48] In order to understand how the substitution of aromatic amino acids can be used to tune the phase transition in our RLPs, a set of new sequences (GGRPSDSXGAPGGGN; designated as RLP-X) was designed, where the central amino acid (X) is either an aromatic residue: tryptophan (W), tyrosine (Y), or phenylalanine (F); or an aliphatic residue: leucine (L), valine (V), or alanine (A).

3.2. Expression and Purification of RLPs

The RLP-X constructs (Figure S1) were expressed following protocols commonly used in the Kiick laboratories.[36,58–60] The composition of the different constructs was determined by amino acid analysis to be within 5% of the expected amino acid composition (Table S1). SDS-PAGE results (Figure S2) confirm the presence of single species for which molecular weight (23.94, 24.27, 24.44, 24.85, 25.04, and 25.32 kDa for the RLP-X sequences where X stands for A, V, L, F, Y, and W respectively) was confirmed by UPLC and ESI-MS (Figure S3) and MALDI-TOF (Figure S4) with a purity greater than 99.9% indicated for all sequences by both methods. Further purification by HPLC was performed on sequences that showed a small amount of impurities in the UPLC, with subsequent analysis via ESI-MS (Figure S3). A comparison between the theoretical molecular weights and those obtained by MALDI-TOF and ESI-MS is shown in Table S2, corroborating the expression of the target RLP sequences. The yield of each RLP construct per liter of cell culture is 30-50 mg. Conformational analysis of the amide peak in FTIR shows that

the amino acid substitutions in the RLP-X constructs have the expected minimal effect on their random coil character, which was indicated to be 75% to 80% in all cases (Figure S5).

3.3. Salt-Induced Phase separation of RLP-Xs

RLP-F/M solutions at 8 mg mL^{-1} were used to assess the effect of different Hofmeister ions in the phase separation of the polypeptide. Stock solutions of 2M sodium chloride (NaCl), ammonium chloride (NH_4Cl), sodium sulfate (Na_2SO_4), and ammonium sulfate ($(NH_4)_2SO_4$) in DI water were prepared and mixed with a concentrated RLP-F/M solution in order to obtain a final RLP concentration of 8 mg mL^{-1} and a final salt concentration of 1.55M. The final ionic strength of each salt solution is 1.55 M for NaCl and NH_4Cl and 4.65 M for Na_2SO_4 and $(NH_4)_2SO_4$. The turbidity of these solutions was measured in a temperature range of 5°C to 85°C to determine the presence of any phase transition (Figure 1A). The polypeptide in the different salts exhibits an LCST-like transition upon heating which is consistent with our previous results.[41,55,64] However, ammonium sulfate was the only salt in these investigations that promoted an UCST-like transition upon cooling (Figure 1A), and was thus used to studyi the phase behavior of all the RLP-X constructs. Ammonium sulfate has been used previously for purifying purposes of the first recombinant RLP sequences[65,66] due to its salting out effect. In the context of the studies of UCST here, interchain interactions (e.g., hydrogen bonding) can be enhanced in the presence of high concentrations of ammonium sulfate,[67,68] which increases the UCST and allows its observation at experimentally accessible temperatures.[69–73] There is minimal information on the temperature-dependence of other interaction modes such as dipolar interactions, ionic interactions, cation-π interactions, π-π contacts, and π-sp^2 interactions, and even less knowledge of how salts affect these interactions. Future research in this area will provide improved understanding of how these interactions are involved in the UCST transition and could thus be tuned to control UCST.

The changes in turbidity of RLP-X solutions (8 mg mL^{-1} in 1.55M ammonium sulfate) show that only the sequences containing aromatic residues (RLP-W, RLP-Y, RLP-F, and RLP-F/M) became turbid, indicative of UCST-like phase separation (Figure 1B). These results are consistent with the literature on proteins such as Fused in Sarcoma (FUS) and LAF-1 RGG, which have aromatic and arginine residues (present in all our constructs) and display UCST-like transitions.[44,46,74,75] It is notable that RLP-W exhibits a transition temperature 15°C higher than those for the phenylalanine and tyrosine analogues (Table 1). Similar transition temperatures of tyrosine and phenylalanine constructs are also somewhat surprising, as other studies have shown reduced LLPS propensity when tyrosine is replaced with phenylalanine,[63,76] though the differences in our observations from these previous reports likely originate from the different solution conditions (ammonium sulfate vs. PBS buffer). Previous computational studies have shown that interactions between arginine and the aromatic amino acids Trp, Tyr, and Phe are possible and favored for Trp.[48,49,77] Recent studies on related RLPs support that arginine interactions are stronger with tryptophan than other aromatic residues.[76] The sequences with aliphatic mutations (RLP-L, RLP-V, and RLP-A) lack any UCST-like transition and exhibit LCST-like transitions only (Figure 1C) which have similar transition temperature values in the three cases, suggesting that the aliphatic mutations have minimal effects on interactions that promote the LCST-like transition in the reported RLPs. We attribute the large increase in absorbance that we observe in the UCST transitions to a homogeneous distribution of larger liquid droplets that form during the coacervation process. In contrast, the LCST transitions of our constructs result in smaller aggregates instead of droplets, and these aggregates tend to precipitate. The distribution of the aggregates in the light path is likely more heterogeneous as well, resulting in the lower turbidity.

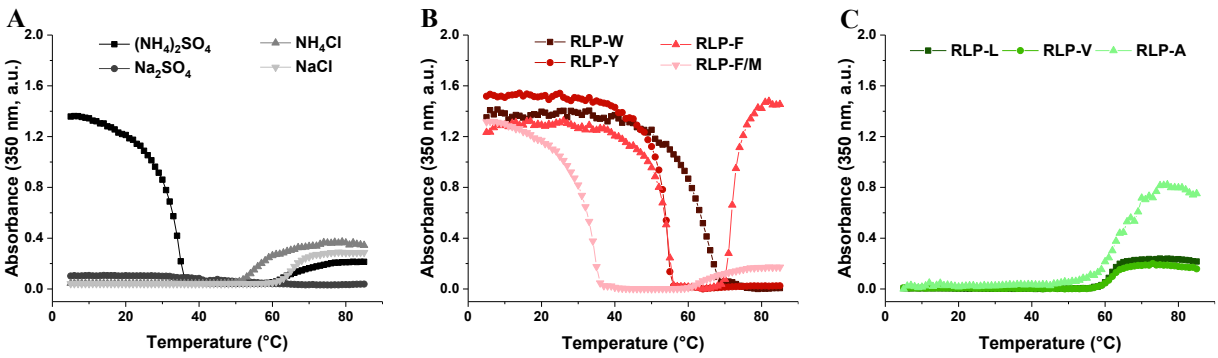

Figure 1. UV-Vis turbidity measurements of RLP-X at 8 mg mL^{-1}. A) RLP-F/M in different salts at 1.55M; ammonium sulfate is the only salt that promotes a UCST-like transition in the polypeptide solution. B) Aromatic RLP-X in ammonium sulfate 1.55M; all the sequences show UCST-like transition. Only the constructs containing Phe have evidence of an LCST-like transition. C) Aliphatic RLP-X in ammonium sulfate 1.55M; no evidence of UCST-like transition is observed. Only LCST-like transitions are evident in these constructs. Only one of three replicates are shown in this figure.

Table1. Transition temperatures of RLP-X in ammonium sulfate 1.55M

	UCST (°C)	LCST (°C)
RLP-W	64.6 ± 5.8	----
RLP-Y	50.3 ± 3.5	----
RLP-F	53.7 ± 0.3	71.8 ± 0.3
RLP-F/M	30.6 ± 2.1	65.8 ± 0.2
RLP-L	----	62.0 ± 0.2
RLP-V	----	62.5 ± 0.4
RLP-A	----	62.8 ± 2.2

3.4. Molecular Level Insight into Interactions of RLP Peptides by Atomistic Simulations

To gain insight into the molecular modes of interactions in the RLP X peptides, we have performed all-atom molecular dynamics (MD) simulations of a 45-residue peptide, (GGRPSDS**X**GA PGGGN)$_3$, with three aromatic (Y, F, W) and three aliphatic (A, L, V) substitutions at the position **X**. The amino acid composition of the simulated peptide is shown in Fig. 2A I for the RLP W peptide and highlights the prevalence of Gly residues. These single-chain simulations were conducted with an explicit solvent model and used a metadynamics-based enhanced sampling technique to facilitate the convergence of equilibrium averages (see methods). As shown in previous work[78], single-chain properties are highly correlated to the protein phase behavior, thereby, supporting the suitability of these simulations for studying the role of different atomic interaction modes in the phase separation propensity. A similar approach was used successfully in our previous work on other proteins of interest to the LLPS community, such as LAF-1 RGG and FUS LC.[46,63]

First, we compute the average number of non-specific contacts (referred to as vdW contacts hereafter) formed between all residue pairs, excluding the ones (i, i+2) which are in close proximity due to bonding constraints, to assess if certain regions of the peptide are more or less prone to interact. As shown in Fig. 2A II for RLP W, the contacts formed between different parts of the peptide chain are relatively well-distributed with both local and non-local interactions present within the equilibrium structural ensemble. As our primary interest is to understand the differences in interactions for different RLP **X** variants, as suggested by the mutagenesis experiments, we also compute the total number of vdW contacts formed between each amino acid type (Figure 2A III). Consistent with the high abundance of glycine residues in the RLP sequence (Figure 2A I), the contact map shows dominant interactions of glycine with itself and other residues. Similarly, other residues such as proline and serine with higher abundance within the simulated sequence also form

higher number of contacts. Such contacts within low-complexity sequences are expected to be invariably present within the protein-rich condensed phases due to the prevalence of specific amino acids and may contribute to the stability of the dense phase.

Next, we want to compare the prevalence of contacts between different residue type pairs independent of the peptide sequence composition. To accomplish this, the contact map values in Figure 2A III were normalized with the maximum number of possible contacts that can be observed between a specific residue pair, based on the sequence composition. The normalized contact maps in Figure 2A IV now show high interaction propensity for the tryptophan residue with itself and with the other residues such as proline and arginine. In addition, a higher number of contacts are also formed between oppositely charged arginine and aspartic acid residues, driven by electrostatic attraction. We present the contact maps for the other RLP X sequences in SI Figure S6, which also highlights the importance of interactions involving aromatic residues. We also see significant interactions between arginine residues, which can be due to the guanidinium ions pairing reported in the literature, further contributing to the stability of the protein-rich phase.

The RLP X constructs show the ability to tune the phase transition behavior form LCST to USCT like phase transitions depending on the identity of residue X. To better understand how the number of contacts formed by each residue are affected by changes in residue X, we calculate the number of vdW contacts formed by each residue with any other residue and normalize it with respect to the number of such residues (X) in the simulated RLP X sequence (Figure 2B). This is akin to summing all the pairwise contacts shown in Figure 2A IV along either of the axis. Notably, all the sequences with aliphatic X substitutions show similar contact propensities for different residues, with only arginine residue showing a slightly higher value, which is also consistent with the pairwise contact maps in SI Figure S6. In contrast, the sequences with aromatic substitutions show

a relatively higher number of contacts formed by the residue X (Figure 2B). Interestingly, more contacts are formed by the tyrosine and tryptophan residues as compared to the phenylalanine, further highlighting differences among the aromatic residues in modulating the phase behavior.

Beyond the sequence-dependent changes, there is also significant interest in understanding the role of atomic interaction modes that are responsible for the observed differences in the contact propensity. Recent work has highlighted the importance of hydrogen bonding, hydrophobic interactions,[46] planar interactions between aromatic π groups,[45] and cation-π interactions (in particular between tyrosine and arginine).[63] As most of these interactions can be captured in modern atomistic simulation models, we compute the number of contacts formed by residue X that can be described as hydrogen bonds, π-π, or cation-π interactions (see methods for calculation details). As shown in Figure 2C, the number of hydrogen bonds formed by the aliphatic residues and phenylalanine are similar and make a relatively modest contribution (~10-13%) toward the observed vdW contacts formed by these residues. The tryptophan and tyrosine residues instead form twice as many hydrogen bonds owing to the presence of hydrogen bond donor/acceptor sidechain atoms (–OH group in Tyr and the –NH group in Trp). In terms of aromatic π-π contacts, tryptophan contacts are formed twice as often as the tyrosine or phenylalanine contacts. Also, tyrosine residues form a higher number of cation-π contacts as compared to the phenyalanine and tryptophan residues. Taken together, this analysis may help explain the differences in the reduced LLPS propensity in mutagenesis experiments when tyrosine residues are replaced with phenylalanine residues due to the loss of sidechain hydrogen bonding and reduced cation-π interactions [74,79]. Our analysis also suggests that tryptophan substitutions should either slightly enhance LLPS or keep it similar to the tyrosine residues, which is consistent with recent work[76].

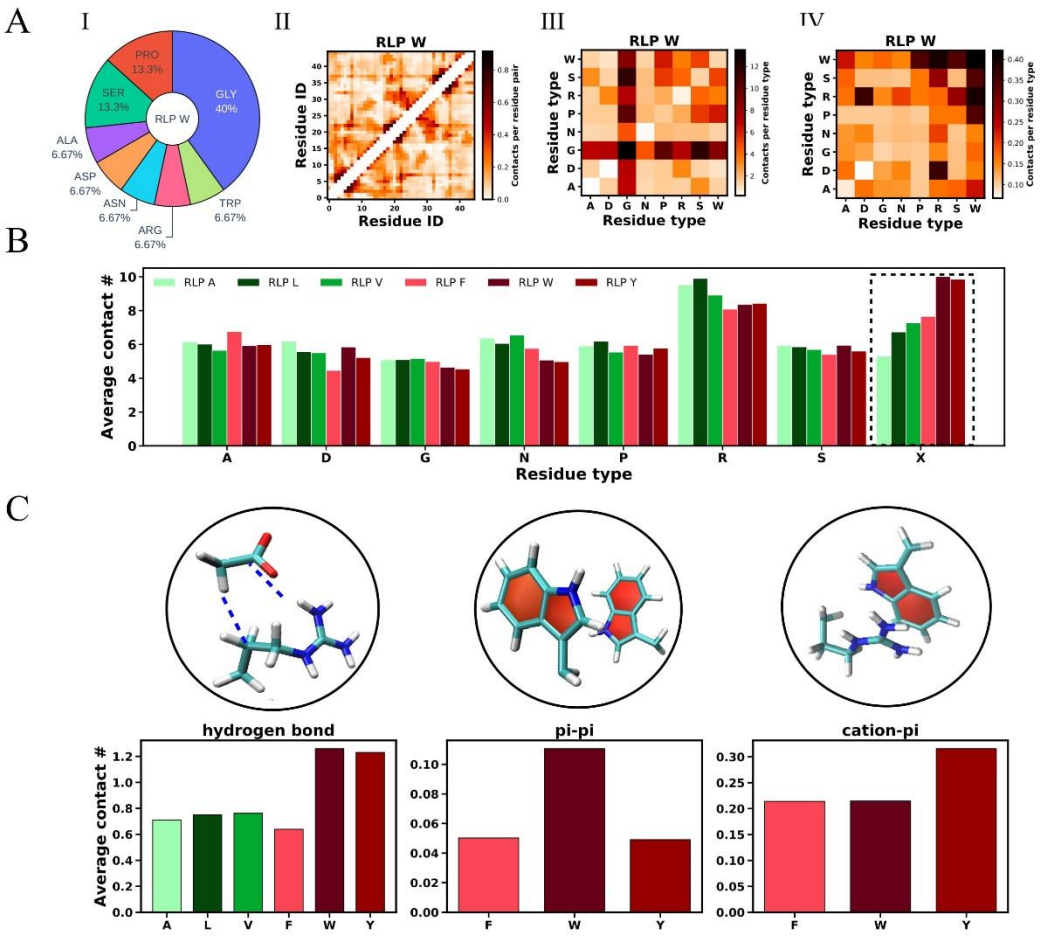

Figure 2. Atomistic intramolecular contacts. A) (I) Amino acid composition of the 45-residue long RLP W peptide that was simulated using an all-atom model (see methods) is shown as a pie chart. (II) The number of average intramolecular VDW contacts formed between each residue pair is plotted as a contact map. The interactions between residues close to each other in the protein sequence (between residues i and i±2) are excluded. (III) The total number of intramolecular VDW contacts formed between each residue type pair is computed based on (II), reflecting the abundance of each pair type in the RLP W sequence. (IV) The contact propensity in (III) is normalized to the number of possible interaction pairs of a given type in the RLP W sequence to obtain insights into their intrinsic interaction strengths. B) The average number of Intramolecular VDW contacts for each residue type normalized to their relative abundance in the RLP X sequence is shown as a

function of residue type. A dashed box highlights the contacts formed by the residue type X substituted by different amino acids (A, L, V, F, W, or Y). C) The number of intramolecular VDW contacts formed by residue type X (A, L, V, F, W, or Y) are further analyzed in terms of important known modes, hydrogen bond, π-π, and cation-π interactions.

3.5. Acrylamide Functionalization Induces LLPS

Polypeptides used for manufacturing hydrogels via photocrosslinking methods generally rely on acrylamide (or acrylate) functionalization, post-purification, to enable subsequent UV-crosslinking.[34,35,80] The effect of such chemical modifications on the phase transitions of the aromatic RLP-X and on the capability of RLP-W to differentiate from its analogue sequences was assessed via turbidimetry assays. N-acryloxysuccinimide was reacted with the lysine residues of the aromatic constructs in order to get RLP-X-Ac as detailed in the experimental section (Figure 3A). The functionalization was confirmed via ^{1}H NMR. The three vinylic peaks between δ 5.65–6.30 ppm[81] confirm the successful functionalization, and comparison of the peaks area to that of the aromatic protons from phenylalanine (δ 7.15–7.40 ppm), tyrosine (δ 6.67, 6.98 ppm), or tryptophan (δ 7.00–7.60 ppm), allowed determination of the degree of acrylamide functionalities on the RLP-X (Figure 3B). The ability of these RLPs to undergo UCST was confirmed at high salt concentrations, (although those concentrations and salt identity are not suitable for applications involving cells), and the transition temperatures showed an increase as the content of acrylamide groups was raised (Figure S7). As the salt concentration was reduced, RLP-W-Ac was the only sequence shown to undergo LLPS in DI water (at all acrylamide contents); LLPS in DI water was observed in the other sequences only for RLP-Y-6Ac and 8Ac and was not observed for RLP-F in any case. These data suggest that the acrylamide functionalization yields sequences prone to LLPS and that tryptophan is a key feature to promote such transitions. The assessments of phase

separation and hydrogel formation were conducted primarily with RLP-W-Ac, because of the higher transition temperature for the RLP-W relative to the other RLP sequences. This resulted in a greater range of conditions that yielded phase separation and a wider range of hydrogel morphologies. RLP-F-Ac was chosen as the non-phase-separating control. The use of the RLP-W--4Ac sample was preferred for further characterization (see below) because the reaction conditions required for producing the 6Ac and 8Ac RLP-W-xAc resulted in the formation of insoluble aggregates during the chemical modification, reducing the amount of total polypeptide recovered after purification.

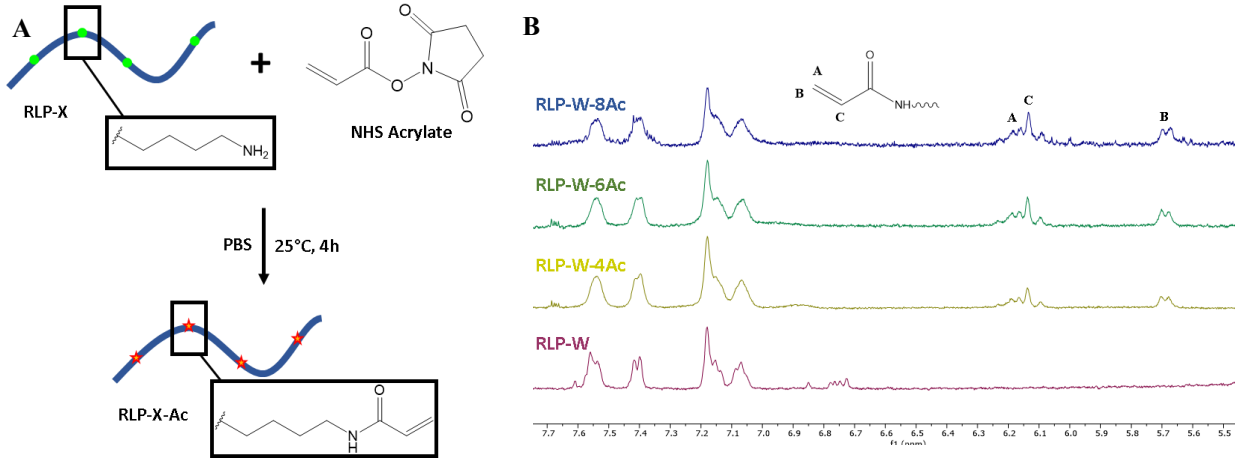

Figure 3. Acrylamide functionalization of RLP-Xs. A) Schematic of functionalization. Amide bound coupling is carried out between the lysine groups of the polypeptide chain and acrylic acid N-hydroxysuccinimide ester. B) NMR spectrum of RLP-W and its functionalized analogues. The vinylic peaks (δ 5.65–6.30 ppm) increase in intesity compared to the tryptophan peaks (δ 7.00–7.60 ppm) as the acrylamide content increases.

3.6. NMR Spectroscopy Reveals RLP-X Specific Amino Acid Interactions

To characterize the possible amino acid interactions responsible of the RLP-W-Ac phase separation, DFQ-COSY and NOESY ^{1}H NMR experiments of soluble (5 mg ml^{-1}, Figures S8 and

S9) and condensed (100 mg mL^{-1}, Figures 4 and S10) samples were performed in a Bruker AVIII 600 MHz NMR spectrometer. Signals that appear in NOESY but not in COSY represent interactions through space due to the tertiary structure and are described here as NOESY-unique signals.

RLP-W and RLP-W-4Ac in solution have NOESY-unique signals of interactions between aromatic tryptophan protons (δ 7.00–7.60 ppm) with Hα tryptophan, (δ 4.60 ppm), Hδ arginine (δ 3.23 ppm), Hα glycine (δ 3.91 ppm), Hβ arginine (δ 1.86 and 1.58 ppm), and Hγ arginine (δ 1.21 ppm) (Figure S8).[82,83] These results suggest tryptophan-tryptophan and tryptophan-arginine spatial proximity consistent with the atomistic simulations reported above (Figure 2A IV). The former interactions are likely to happen through π-π interactions and the later through cation-π and hydrogen bonding interactions as shown in Figure 2C and in accordance with reports of similar interactions between arginine and tyrosine in other IDPs such as FUS and LAF-1.[44,46,74,75] RLP-F and RLP-F-4Ac samples show NOESY-unique signals between the phenylalanine aromatic protons (δ 7.15–7.40 ppm) and Hα and Hβ from phenylalanine (δ 3.00, 3.15, 4.56 ppm; Figure S9)[82,83] which is consistent with the our computational studies where phenylalanine has the most contacts with itself (Figure S6E IV) and are more likely to happen through π-π interactions (Figure 2C).

For the NMR studies of condensed samples, a higher concentration (100 mg mL^{-1}) of RLP-W and RLP-W-4Ac was used. The samples were allowed to phase separate and both the top (RLP-poor) and bottom (RLP-rich) phases were characterized. Figures 4 shows the NMR spectra of the RLP-rich phase. The COSY spectra reveals protons less than three-chemical bonds away in the tryptophan aromatic region for RLP W and RLP-W-4Ac (δ 7.00–7.60 ppm; Figures 4A and 4B) and in the acrylamide vinylic region for RLP-W-4Ac (δ 5.65–6.30 ppm; Figure 4B). Meanwhile

the NOESY spectra reveals the same unique signals described above for the soluble samples but with higher intensity (Figures 4C and 4D). Interestingly, new sets of NOESY-unique signals in RLP-W-4Ac reveal acrylamide protons interactions (δ 5.65–6.30 ppm) with aromatic tryptophan protons (δ 7.00–7.60 ppm) and Hβ arginine (δ 1.86 and 1.58 ppm) (Figure 4D, dashed boxes).[82,83] These results suggest that the acrylamide groups interact with both the aromatic ring of tryptophan and the arginine potentially through aromatic-sp^2 and sp^2-sp^2 contacts.[46,75] and support the results observed in the phase diagrams in Figure S7, where the inclusion of acrylamide functionalities promotes the increment of RLP-W transition temperatures. The NMR spectra of RLP-poor phases of RLP-W and RLP-W-4Ac (Figure S10), show low intensity signals in the same region, consistent with the 5 mg ml^{-1} samples (Figure S8) and the much lower RLP concentration expected in the RLP-poor phases.

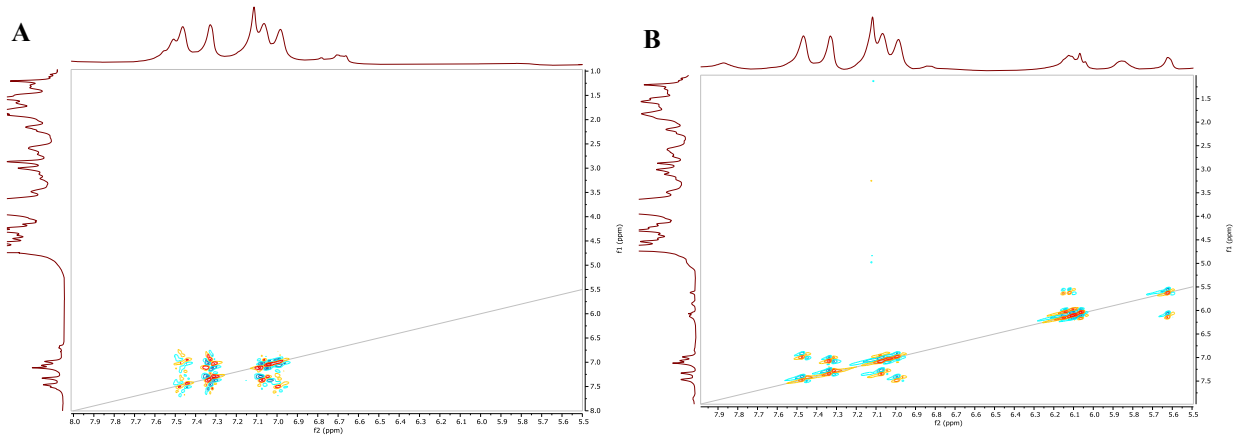

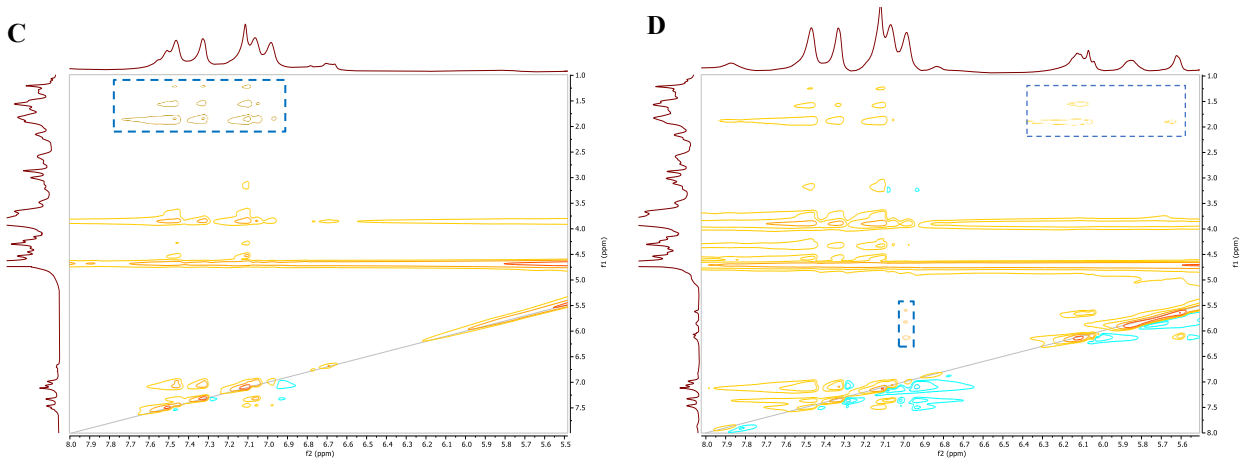

Figure 4. COSY and NOESY spectra of RLP W and RLP W-4Ac. A, B) 2D-COSY spectrum of RLP W (A) and RLP-W-4Ac (B). Cross peaks show that the aromatic protons observed in NOESY belong to a same tryptophan (A, B) and the same acrylamide (B). C) 2D-NOESY spectrum of RLP W. Cross peaks between 1 to 5 ppm suggest interactions between tryptophan aromatic rings with other tryptophan, glycine, and arginine residues. D) 2D-NOESY spectrum of RLP-W-4Ac. Besides the interactions described in (C), interactions between acrylamide protons with arginine and tryptophan are suggested. The blue boxes show regions where the intensity had to be increased to observe the cross peak.

3.7. RLP-W-Ac Undergoes Phase Separation in PBS

While the acrylamide groups in RLP-W-Ac induce LLPS in water potentially through sp^2 interactions with tryptophan and arginine, buffers such as PBS are needed for maintaining a suitable environment in cell culture applications. Because PBS contains ca. 150mM NaCl and this salt is known to promote the solubility of RLPs,[41] the phase separation capabilities of the acrylamide-functionalized polypeptide under conditions suitable for cell culture hydrogels was tested. While the trends in phase separation temperatures determined via turbidity were determined with 0.8 wt% RLP solutions for comparisons with literature reports,[12,41] polypeptide concentrations of at least 8.8 wt% (88 mg mL^{-1}) are essential for effective interchain crosslinking

of RLPs, so our additional characterization of phase separation and hydrogel formation was conducted at higher concentrations.[84] A phase diagram of temperature vs. composition of RLP-W-4Ac in PBS was therefore generated (Figure 5A). The coexistence curve was constructed from turbidity measurements of RLP-W-4Ac dissolved in PBS in a range of concentrations from 20 wt% to 0.8 wt%, upon cooling from 85°C to 5°C, and was complemented with the equilibrium concentrations of phase separated RLP-W-4Ac solutions (overnight at room temperature and 4°C) at initial concentrations of 5 and 10 wt%. These equilibrium concentrations were determined from the top and bottom phases via quantitative NMR using an internal standard as reference and can be found in Table 2.

Table 2. Equilibrium concentrations of RLP-W-4Ac in PBS

Initial conc. (wt%)	Temperature (°C)	Top phase (wt%)	Bottom phase (wt%)
10	25	1.9 ± 0.1	23.6 ± 0.2
10	4	0.8 ± 0.1	27.2 ± 1.1
5	4	0.2 ± 0.1	26.6 ± 2.4

As presented in Figure 5A, the UCST of RLP-W-4Ac ranges from 18.8 ± 2.1°C at low concentrations (0.8 wt%) to 46.6 ± 3.7°C at higher concentrations (10 wt%), and 33.6 ± 0.2°C at concentrations of 20 wt%. The equilibrium concentrations at 25°C complement the phase coexistence curve obtained by turbidimetry measurements, while the equilibrium concentrations at 4°C show that a minimum of 0.2 wt% and no more than 27.2 wt% of RLP-W-4Ac in PBS are required for observing phase separation above freezing. The RLP-rich phase, isolated after macroscale phase separation overnight, forms a continuous hydrogel upon crosslinking, while the RLP-poor phase fails to form hydrogels. These observations suggest that in the microstructured RLP hydrogels (see below), it is only the higher-concentration RLP phase that comprises a

crosslinked, percolated polymer network. As expected, the phase diagram (Figure 5A) has the typical shape of a polymer with UCST transition[85] and is consistent with other proteins that undergo LLPS upon cooling as is the case of γ-crystallins[86,87] or other RLP constructs.[76,88] Interestingly, in such proteins, the LLPS transition is enhanced with increasing the content of both arginine and aromatic amino acids as we have shown here in our atomistic simulations (Figure 2A). The transition temperatures shown in the coexistence curve suggest conditions suitable for cell culture applications, as the solutions phase separate close to physiological conditions and at concentrations required for effective crosslinking as detailed above.

3.8. Control of Phase Separation Modulates Microstructure and Macroscale Mechanical Properties of Hydrogels

To optimize the properties of these materials for cell encapsulation, both the microstructure and mechanical properties should be tunable depending on the application and cell requirements. By employing the phase diagram (Figure 5A) as a guide, conditions under which the RLP-W-4Ac solution will phase separate can be selected, and the microstructure generated during LLPS can be arrested during photo-crosslinking. In order to generate more stable emulsions, a heating-cooling protocol (Figure 5B) was developed, based on literature precedent showing that such treatment can favor formation of bicontinuous structures that jam the system and delay the phase separation.[89–92] To assess such affects in the RLP hydrogels, the RLP-W-4Ac emulsions were warmed above the transition temperature (80°C and 60°C) and immediately cooled for 30 seconds in an ice bath. The final temperatures were determined from the cooling profiles (Figure S11), and were 19.5 ± 0.95 °C and 15.1 ± 0.5 °C, respectively. Completely opaque hydrogels were obtained upon UV crosslinking. RLP-F-4Ac was used as a non-microstructured control; these solutions were always transparent at any temperature when warmed for fewer than 45 seconds.

Two types of morphologies can be observed in Figure 5C for RLP-W-4Ac (20 wt%, 80°C): buffer spherical domains, characteristic of nucleation and growth (black circles in Figure 5C) dispersed in an RLP-rich matrix (white signal surrounding the black circles in Figure 5C) and, inside the large buffer domain, a dispersed RLP-rich network with a structure akin to that of spinodal decomposition induced by the quenching process.[89–92] RLP-W-4Ac (20 wt%, 60°C) resulted in different morphological features: spherical RLP-rich domains dispersed in the RLP network (Figure 5E), perhaps formed by a percolation-to-cluster mechanism where bicontinuous domains break, forming stable spheres.[93–95] The bicontinuous networks shown in Figures 5C and 5E can be better observed in the 3D projection of the complete z-stack in Figure S12. In contrast, both 80°C and 60°C RLP-F-4Ac 20 wt% samples show no microstructure at all (Figures 5D and 5F) which was expected owing to the lack of a UCST transition for this construct. These confocal results confirm not only that tryptophan substitutions are essential to generate microstructures in RLP hydrogels but also the thermal treatment of the precursor emulsions can be easily exploited to generate different hydrogel microstructures.

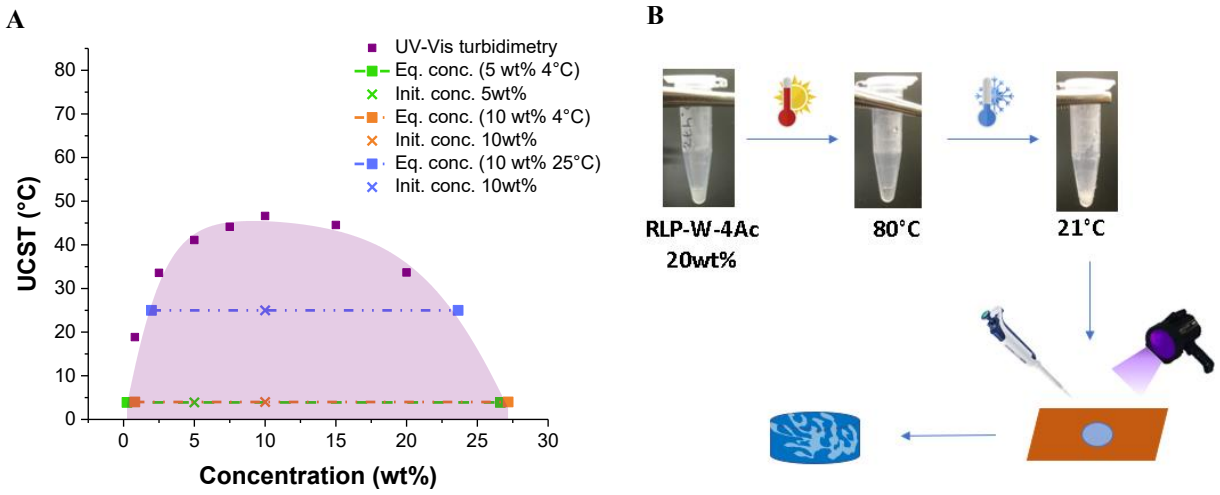

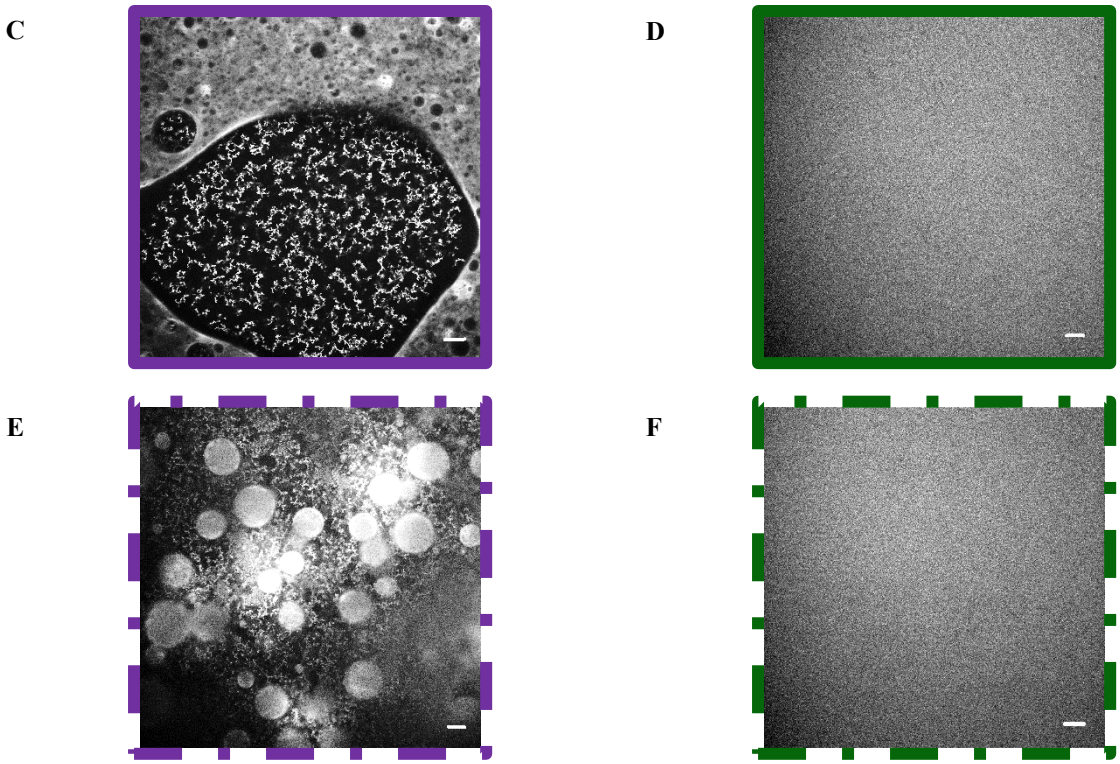

Figure 5. Hydrogel formation and characterization. A) The transition temperatures of RLP-W-4Ac are close to physiological conditions in a range of concentration of 0.8 to 20 wt%. The phase diagram was complemented with equilibrium concentrations measured of completely phase-separated emulsions through quantitative H^1 NMR with an internal reference. B) Schematic of hydrogel formation by heating-cooling protocol. C, D) Autofluorescence images of photo-crosslinked RLP-W-4Ac 20wt% (C) and RLP-F-4Ac 20 wt% (D) cooling from 80°C. E, F) Autofluorescence images of photo-crosslinked RLP-W-4Ac 20wt% (E) and RLP-F-4Ac 20 wt% (F) cooling from 60°C. The white signal corresponds to the RLP-rich phase. Scale bar 20 µm.

The impact of the microstructure on the hydrogel mechanical behavior was preliminarily evaluated by in situ crosslinking of the emulsions in a rheometer. All samples for both microscopy and rheometry were heated and cooled before loading into the rubber mold or onto the rheometer, respectively. In both cases, the time that elapses prior to the start of UV crosslinking is 30 to 40

seconds. This reproducibility of the 'lag' time between the mixing and the crosslinking of the various samples (in both microscopy and rheometry) allows us to compare the relative differences in hydrogel structure and their potential contribution to rheological properties. The storage modulus (G') of RLP-W-4Ac and RLP-F-4Ac hydrogels (Figure 6), shows a concentration dependance common in hydrogels.[96,97] However, the G' for the RLP-W-4Ac (80°C) samples is always lower than the G' for RLP-F-4Ac (80°C) at the same concentration (e.g., 92, 47.7, and 55.5 % lower at 10, 15, and 20 wt% respectively). In regard to the cooling gradients, Figure 6A reveals that G' for RLP-W-4Ac (60°C) is 87.5% lower compared to the 80°C sample at 15 wt% and 58% lower at 20 wt%. Since the RLP-W-4Ac 20wt% (60°C) comprises largely RLP spherical domains (rather than in a continuous network) (Figure 5E), the decrease in the shear storage modulus of the bulk hydrogel suggests that these spherical domains do not contribute substantially to the mechanical properties of the network. In contrast, RLP-F-4Ac samples are independent of the thermal treatment with no more than 5% difference in G' for any case (Figure 6B); this behavior is consistent with the lack of microstructure (Figures 5D and 5F).

The microstructure-mechanical correlation is consistent with that expected from poroelastic constitutive behavior, a model describing a system where a fluid flows through a viscoelastic porous solid. The permeability of the network, can be determined from the effective pore size, and is related to the square of a characteristic length scale, typically the fiber diameter.[98] For the purposes of this discussion, because the RLP concentration is the same across the comparison samples here, hydrogels comprising RLP regions with smaller dimensions should yield smaller pore sizes, and hence would be expected to show lower permeability. The mechanical behavior of hydrogels is inversely proportional to the permeability of the system, because the viscous performance of the solvent is intrinsically related to such permeability. Thus, the higher the

permeability, the closer the mechanical performance of the hydrogel is to that of water.[98,102] RLP-F-4Ac, being a homogeneous system, has 'fiber' diameters at a molecular dimension, making the permeability so small that the overall mechanical behavior is that of a purely viscoelastic system. In contrast, RLP-W-4Ac should show permeability comprising that of the continuous RLP molecular network of the crosslinked hydrogel phases, and also that of the microscale phase which itself is percolated and is a main contribution to the mechanical integrity of the microstructured, 'bulk' hydrogels. Since the permeability in RLP-W-4Ac would thus be expected to be greater than that of RLP-F-4Ac, it is consistent that the mechanical performance of the RLP-W-4Ac is lower. Future results to experimentally determine permeability (via methods such as cavitation[99] and nano- and micro-indentation[100,101] methods) will enable a more quantitative treatment of the RLP hydrogel permeability and its relationship to observed mechanical properties.

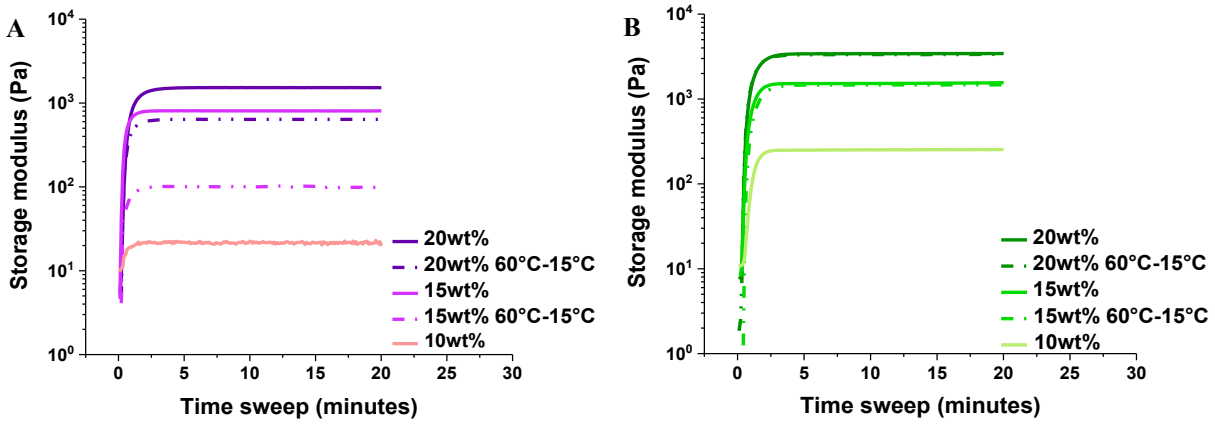

Figure 6. Mechanical characterization of hydrogels. Time sweeps of hydrogels made of RLP W-4Ac (A) and RLP-F-4Ac (B) at different concentrations. Two different cooling treatments of precursors are represented: from 80°C (solid lines) and from 60°C (dotted lines).

Interestingly , the materials here shown develop similar bicontinuous microstructures to those reported in hydrogels based on ELPs,[24,103–105] where the characteristic LCST transition is used for promoting the microstructure formation with pH,[24] temperature,[24,103,104] or amino acid charge density changes[105] as the handles to control the process. Although our approach has similarities with the strategies reported in these bicontinuous ELP hydrogels, such as phase transition control through sequence design and temperature-induced generation of microstructure, our approaches are slightly different in that they do not require partial chemical crosslinking before phase separation,[24] the inclusion of order-inducing domains that connect ELP aggregates,[103,104] or the inclusion of charged blocks to drive assembly from micelles to interconnected networks.[105] The correlation of mechanical behavior with microstructural features of our materials are consistent with those previously reported; overall, the storage modulus increases as the expected permeability decreases. While the hydrogels in the present report exhibit continuous biopolymer phases that are generally not observed the ELP-based hydrogels, both the RLP materials we report and the previous ELP materials exhibit shear storage moduli of ~1-4 kPa (or greater when stabilized with order-inducing structures (~12 kPa)).[103] This type of polypeptide-based microstructured materials have been proven to be successful in drug delivery systems[24] and as injectable scaffolds with rapid tissue integration.[103] Similar applications are expected for the materials reported here.

4. Conclusions

We investigate the impact of amino acid mutations on the microstructure formation of RLP-X hydrogels, where various substitutions are made in the X position in order to modify the ability of the RLPs to phase separate. Experimental evidence indicates that the aromatic moieties are more prone to promote UCST and that tryptophan is more potent than tyrosine and phenylalanine, which show similar behavior in ammonium sulfate. The types and number of interactions of the aromatic

residues with other residues in the polypeptide chain have been elucidated via atomistic simulations. The simulations show that tyrosine, tryptophan, and arginine have a higher propensity to form contacts than the other residue types, and that these contacts involve hydrogen bonding and π-π contacts both of which are occur to a greater extent for Tyr and Trp over Phe. The simulations also suggest that Tyr can form more cation- π contacts than the other two aromatic residues, highlighting the importance of arginine and tyrosine interactions, as proposed in the recent literature.

The functionalization of the RLP-X constructs with acrylamide groups further promotes the LLPS of the polypeptides, potentially by π-sp^2 interactions with tryptophan and sp^2-sp^2 interactions with arginine, which makes both tryptophan and acrylamide functionalities good candidates for adjusting the phase transition of RLP-hydrogel precursors in PBS solutions into physiologically relevant temperature windows. In demonstration of this possibility, microstructured hydrogels were produced from RLP-W-4Ac emulsions in PBS; the morphology and mechanical performance of the hydrogels are correlated and can be tuned by the cooling gradients and duration of phase separation of the hydrogel precursors prior to photocrosslinking. Overall, our results demonstrate that amino acid substitutions and chemical modifications of RLPs can be used to tune their UCST, which in turn can be synergistically combined with variations in cooling gradients and other processing conditions to tune the final microstructure and mechanical properties of RLP-based hydrogels.

Supporting Information

The following Supporting Information is available free of charge at the ACS website.

Figure S1. RLP-X sequence; Figure S2. SDS-PAGE of purified RLP-X sequences; Figure S3. UPLC and ESI-MS spectra of the RLP-X sequences; Figure S4. MALDI-TOF of the RLP-X

sequences; Figure S5. Structural analysis of the RLP-X constructs; Figure S6. Atomistic intramolecular contacts; Figure S7. Phase diagrams of the aromatic RLP-X as a function of increasing concentration of ammonium sulfate; Figure S8. 2D NOESY and COSY NMR spectra of RLP-W and RLP-W-4Ac in solution; Figure S9. 2D NOESY and COSY NMR spectra of RLP-F and RLP-F-4Ac in solution; Figure S10. 2D NOESY and COSY NMR spectra of the top solution of phase separated RLP-W and RLP-W-4Ac; Figure S11. Cooling profiles of RLP-W-4Ac solutions; Table S1. Amino composition of the RLP-X sequences; Table S2. Molecular weights in Da of the RLP-X sequences.

Corresponding Author

*Phone: +1 302-831-0201. E-mail: kiick@udel.edu.

Notes

The authors declare no competing financial interest.

Acknowledgements

The authors gratefully acknowledge support from the National Science Foundation (DMR-1609544 (UD) and DMR-2004796 (UD and Lehigh University)). Atomistic simulations were made possible by the high-performance computing capabilities of the Extreme Science and Engineering Discovery Environment (XSEDE), which is supported by the NSF grant TG-MCB-120014. Instrument resources from the Delaware COBRE program were supported by grants from the National Institute of General Medical Sciences (1-P30-GM110758-01 and 1-P20-RR017716). We also thank the Delaware Biotechnology Institute Bio-Imaging Center for access to microscopy equipment that was supported by a shared instrumentation grant (S10 OD016361) and the Delaware INBRE grant from NIH-NIGMS (P20 GM103446). The views represented are those of the authors and do not necessarily reflect those of the funding institutions.

References

(1) Anfinsen, C. B. Principles That Govern the Folding of Protein Chains. *Science (80-.).* **1973**, *181*, 223–230, DOI: 10.1126/science.181.4096.223.

(2) Baskakov, I. V.; Kumar, R.; Srinivasan, G.; Ji, Y.; Bolen, D. W.; Thompson, E. B. Trimethylamine N -Oxide-Induced Cooperative Folding of an Intrinsically Unfolded Transcription-Activating Fragment of Human Glucocorticoid Receptor. *J. Biol. Chem.* **1999**, *274*, 10693–10696, DOI: 10.1074/jbc.274.16.10693.

(3) Bielska, A. A.; Zondlo, N. J. Hyperphosphorylation of Tau Induces Local Polyproline II Helix †. *Biochemistry* **2006**, *45*, 5527–5537, DOI: 10.1021/bi052662c.

(4) Brister, M. A.; Pandey, A. K.; Bielska, A. A.; Zondlo, N. J. OGlcNAcylation and Phosphorylation Have Opposing Structural Effects in Tau: Phosphothreonine Induces Particular Conformational Order. *J. Am. Chem. Soc.* **2014**, *136*, 3803–3816, DOI: 10.1021/ja407156m.

(5) Uversky, V. N.; Davé, V.; Iakoucheva, L. M.; Malaney, P.; Metallo, S. J.; Pathak, R. R.; Joerger, A. C. Pathological Unfoldomics of Uncontrolled Chaos: Intrinsically Disordered Proteins and Human Diseases. *Chem. Rev.* **2014**, *114*, 6844–6879, DOI: 10.1021/cr400713r.

(6) Courchaine, E. M.; Lu, A.; Neugebauer, K. M. Droplet Organelles? *EMBO J.* **2016**, *35*, 1603–1612, DOI: 10.15252/embj.201593517.

(7) Mao, Y. S.; Zhang, B.; Spector, D. L. Biogenesis and Function of Nuclear Bodies. *Trends Genet.* **2011**, *27*, 295–306, DOI: 10.1016/j.tig.2011.05.006.

(8) Rabouille, C. Membraneless Organelles in Cell Biology. *Traffic* **2019**, *20*, 885–886, DOI: 10.1111/tra.12686.

(9) Lin, Y.; Protter, D. S. W.; Rosen, M. K.; Parker, R. Formation and Maturation of Phase-Separated Liquid Droplets by RNA-Binding Proteins. *Mol. Cell* **2015**, *60*, 208–219, DOI: 10.1016/j.molcel.2015.08.018.

(10) Molliex, A.; Temirov, J.; Lee, J.; Coughlin, M.; Kanagaraj, A. P.; Kim, H. J.; Mittag, T.; Taylor, J. P. Phase Separation by Low Complexity Domains Promotes Stress Granule Assembly and Drives Pathological Fibrillization. *Cell* **2015**, *163*, 123–133, DOI: 10.1016/j.cell.2015.09.015.

(11) Boeynaems, S.; Alberti, S.; Fawzi, N. L.; Mittag, T.; Polymenidou, M.; Rousseau, F.; Schymkowitz, J.; Shorter, J.; Wolozin, B.; Van Den Bosch, L.; Tompa, P.; Fuxreiter, M. Protein Phase Separation: A New Phase in Cell Biology. *Trends Cell Biol.* **2018**, *28*, 420–435, DOI: 10.1016/j.tcb.2018.02.004.

(12) Quiroz, F. G.; Chilkoti, A. Sequence Heuristics to Encode Phase Behaviour in Intrinsically Disordered Protein Polymers. *Nat. Mater.* **2015**, *14*, 1164–1171, DOI: 10.1038/nmat4418.

(13) Franzmann, T. M.; Jahnel, M.; Pozniakovsky, A.; Mahamid, J.; Holehouse, A. S.; Nüske, E.; Richter, D.; Baumeister, W.; Grill, S. W.; Pappu, R. V; Hyman, A. A.; Alberti, S. Phase Separation of a Yeast Prion Protein Promotes Cellular Fitness. *Science (80-.).* **2018**, *359*, eaao5654, DOI: 10.1126/science.aao5654.

(14) Rayman, J. B.; Karl, K. A.; Kandel, E. R. TIA-1 Self-Multimerization, Phase Separation, and Recruitment into Stress Granules Are Dynamically Regulated by Zn 2+. *Cell Rep.* **2018**, *22*, 59–71, DOI: 10.1016/j.celrep.2017.12.036.

(15) Smith, J.; Calidas, D.; Schmidt, H.; Lu, T.; Rasoloson, D.; Seydoux, G. Spatial Patterning of P

Granules by RNA-Induced Phase Separation of the Intrinsically-Disordered Protein MEG-3. *Elife* **2016**, *5*, 1–19, DOI: 10.7554/eLife.21337.

(16) Reed, E. H.; Hammer, D. A. Redox Sensitive Protein Droplets from Recombinant Oleosin. *Soft Matter* **2018**, *14*, 6506–6513, DOI: 10.1039/C8SM01047A.

(17) Schuster, B. S.; Reed, E. H.; Parthasarathy, R.; Jahnke, C. N.; Caldwell, R. M.; Bermudez, J. G.; Ramage, H.; Good, M. C.; Hammer, D. A. Controllable Protein Phase Separation and Modular Recruitment to Form Responsive Membraneless Organelles. *Nat. Commun.* **2018**, *9*, 2985, DOI: 10.1038/s41467-018-05403-1.

(18) Jo, Y.; Jung, Y. Interplay between Intrinsically Disordered Proteins inside Membraneless Protein Liquid Droplets. *Chem. Sci.* **2020**, *11*, 1269–1275, DOI: 10.1039/C9SC03191J.

(19) Costa, S. A.; Simon, J. R.; Amiram, M.; Tang, L.; Zauscher, S.; Brustad, E. M.; Isaacs, F. J.; Chilkoti, A. Photo-Crosslinkable Unnatural Amino Acids Enable Facile Synthesis of Thermoresponsive Nano- to Microgels of Intrinsically Disordered Polypeptides. *Adv. Mater.* **2018**, *30*, 1704878, DOI: 10.1002/adma.201704878.

(20) Ibáñez-Fonseca, A.; Flora, T.; Acosta, S.; Rodríguez-Cabello, J. C. Trends in the Design and Use of Elastin-like Recombinamers as Biomaterials. *Matrix Biol.* **2019**, *84*, 111–126, DOI: 10.1016/j.matbio.2019.07.003.

(21) Roberts, S.; Dzuricky, M.; Chilkoti, A. Elastin-like Polypeptides as Models of Intrinsically Disordered Proteins. *FEBS Lett.* **2015**, *589*, 2477–2486, DOI: 10.1016/j.febslet.2015.08.029.

(22) Al-Husini, N.; Tomares, D. T.; Bitar, O.; Childers, W. S.; Schrader, J. M. α-Proteobacterial RNA Degradosomes Assemble Liquid-Liquid Phase-Separated RNP Bodies. *Mol. Cell* **2018**, *71*, 1027-1039.e14, DOI: 10.1016/j.molcel.2018.08.003.

(23) Ma, Q.; Song, Y.; Sun, W.; Cao, J.; Yuan, H.; Wang, X.; Sun, Y.; Shum, H. C. Cell-Inspired All-Aqueous Microfluidics: From Intracellular Liquid–Liquid Phase Separation toward Advanced Biomaterials. *Adv. Sci.* **2020**, *7*, 1903359, DOI: 10.1002/advs.201903359.

(24) Wang, H.; Paul, A.; Nguyen, D.; Enejder, A.; Heilshorn, S. C. Tunable Control of Hydrogel Microstructure by Kinetic Competition between Self-Assembly and Crosslinking of Elastin-like Proteins. *ACS Appl. Mater. Interfaces* **2018**, *10*, 21808–21815, DOI: 10.1021/acsami.8b02461.

(25) LeSavage, B. L.; Suhar, N. A.; Madl, C. M.; Heilshorn, S. C. Production of Elastin-like Protein Hydrogels for Encapsulation and Immunostaining of Cells in 3D. *J. Vis. Exp.* **2018**, No. 135, 1–11, DOI: 10.3791/57739.

(26) Inostroza-Brito, K. E.; Collin, E.; Siton-Mendelson, O.; Smith, K. H.; Monge-Marcet, A.; Ferreira, D. S.; Rodríguez, R. P.; Alonso, M.; Rodríguez-Cabello, J. C.; Reis, R. L.; Sagués, F.; Botto, L.; Bitton, R.; Azevedo, H. S.; Mata, A. Co-Assembly, Spatiotemporal Control and Morphogenesis of a Hybrid Protein–Peptide System. *Nat. Chem.* **2015**, *7*, 897–904, DOI: 10.1038/nchem.2349.

(27) Gonzalez, M. A.; Simon, J. R.; Ghoorchian, A.; Scholl, Z.; Lin, S.; Rubinstein, M.; Marszalek, P.; Chilkoti, A.; López, G. P.; Zhao, X. Strong, Tough, Stretchable, and Self-Adhesive Hydrogels from Intrinsically Unstructured Proteins. *Adv. Mater.* **2017**, *29*, 1604743, DOI: 10.1002/adma.201604743.

(28) Liu, L.; Wang, H.; Han, Y.; Lv, S.; Chen, J. Using Single Molecule Force Spectroscopy to Facilitate a Rational Design of Ca 2+ -Responsive β-Roll Peptide-Based Hydrogels. *J. Mater. Chem. B* **2018**, *6*, 5303–5312, DOI: 10.1039/C8TB01511B.

(29) Bulutoglu, B.; Yang, S. J.; Banta, S. Conditional Network Assembly and Targeted Protein Retention via Environmentally Responsive, Engineered β-Roll Peptides. *Biomacromolecules* **2017**, *18*, 2139–2145, DOI: 10.1021/acs.biomac.7b00457.

(30) Frey, S.; Richter, R. P.; Gorlich, D. FG-Rich Repeats of Nuclear Pore Proteins Form a Three-Dimensional Meshwork with Hydrogel-Like Properties. *Science.* **2006**, *314*, 815–817, DOI: 10.1126/science.1132516.

(31) Li, L.; Kiick, K. L. Resilin-Based Materials for Biomedical Applications. *ACS Macro Lett.* **2013**, *2*, 635–640, DOI: 10.1021/mz4002194.

(32) Whittaker, J. L.; Dutta, N. K.; Elvin, C. M.; Choudhury, N. R. Fabrication of Highly Elastic Resilin/Silk Fibroin Based Hydrogel by Rapid Photo-Crosslinking Reaction. *J. Mater. Chem. B* **2015**, *3*, 6576–6579, DOI: 10.1039/C5TB00970G.

(33) Luo, F.; Qian, Z.-G.; Xia, X.-X. Responsive Protein Hydrogels Assembled from Spider Silk Carboxyl-Terminal Domain and Resilin Copolymers. *Polymers (Basel).* **2018**, *10*, 915, DOI: 10.3390/polym10080915.

(34) Lau, H. K.; Paul, A.; Sidhu, I.; Li, L.; Sabanayagam, C. R.; Parekh, S. H.; Kiick, K. L. Microstructured Elastomer-PEG Hydrogels via Kinetic Capture of Aqueous Liquid-Liquid Phase Separation. *Adv. Sci.* **2018**, *5*, 1701010, DOI: 10.1002/advs.201701010.

(35) Lau, H. K.; Rattan, S.; Fu, H.; Garcia, C. G.; Barber, D. M.; Kiick, K. L.; Crosby, A. J. Micromechanical Properties of Microstructured Elastomeric Hydrogels. *Macromol. Biosci.* **2020**, *20*, 1900360, DOI: 10.1002/mabi.201900360.

(36) Charati, M. B.; Ifkovits, J. L.; Burdick, J. A.; Linhardt, J. G.; Kiick, K. L. Hydrophilic Elastomeric Biomaterials Based on Resilin-like Polypeptides. *Soft Matter* **2009**, *5*, 3412, DOI: 10.1039/b910980c.

(37) Li, L.; Stiadle, J. M.; Lau, H. K.; Zerdoum, A. B.; Jia, X.; Thibeault, S. L.; Kiick, K. L. Tissue Engineering-Based Therapeutic Strategies for Vocal Fold Repair and Regeneration. *Biomaterials* **2016**, *108*, 91–110, DOI: 10.1016/j.biomaterials.2016.08.054.

(38) McGann, C. L.; Levenson, E. A.; Kiick, K. L. Resilin-Based Hybrid Hydrogels for Cardiovascular Tissue Engineering. *Macromol. Chem. Phys.* **2013**, *214*, 203–213, DOI: 10.1002/macp.201200412.

(39) Kim, Y.; Gill, E. E.; Liu, J. C. Enzymatic Cross-Linking of Resilin-Based Proteins for Vascular Tissue Engineering Applications. *Biomacromolecules* **2016**, *17*, 2530–2539, DOI: 10.1021/acs.biomac.6b00500.

(40) Broide, M. L.; Tominc, T. M.; Saxowsky, M. D. Using Phase Transitions to Investigate the Effect of Salts on Protein Interactions. *Phys. Rev. E* **1996**, *53*, 6325–6335, DOI: 10.1103/PhysRevE.53.6325.

(41) Li, L.; Luo, T.; Kiick, K. L. Temperature-Triggered Phase Separation of a Hydrophilic Resilin-Like Polypeptide. *Macromol. Rapid Commun.* **2015**, *36*, 90–95, DOI: 10.1002/marc.201400521.

(42) Da Vela, S.; Exner, C.; Schäufele, R. S.; Möller, J.; Fu, Z.; Zhang, F.; Schreiber, F. Arrested and Temporarily Arrested States in a Protein–Polymer Mixture Studied by USAXS and VSANS. *Soft Matter* **2017**, *13*, 8756–8765, DOI: 10.1039/C7SM01434A.

(43) Dignon, G. L.; Zheng, W.; Kim, Y. C.; Mittal, J. Temperature-Controlled Liquid–Liquid Phase Separation of Disordered Proteins. *ACS Cent. Sci.* **2019**, *5*, 821–830, DOI: 10.1021/acscentsci.9b00102.

(44) Brangwynne, C. P.; Tompa, P.; Pappu, R. V. Polymer Physics of Intracellular Phase Transitions. *Nat. Phys.* **2015**, *11*, 899–904, DOI: 10.1038/nphys3532.

(45) Vernon, R. M.; Chong, P. A.; Tsang, B.; Kim, T. H.; Bah, A.; Farber, P.; Lin, H.; Forman-Kay, J. D. Pi-Pi Contacts Are an Overlooked Protein Feature Relevant to Phase Separation. *Elife* **2018**, *7*, 1–48, DOI: 10.7554/eLife.31486.

(46) Murthy, A. C.; Dignon, G. L.; Kan, Y.; Zerze, G. H.; Parekh, S. H.; Mittal, J.; Fawzi, N. L. Molecular Interactions Underlying Liquid−liquid Phase Separation of the FUS Low-Complexity Domain. *Nat. Struct. Mol. Biol.* **2019**, *26*, 637–648, DOI: 10.1038/s41594-019-0250-x.

(47) Nandi, C. L.; Singh, J.; Thornton, J. M. Atomic Environments of Arginine Side Chains in Proteins. *"Protein Eng. Des. Sel.* **1993**, *6*, 247–259, DOI: 10.1093/protein/6.3.247.

(48) Gallivan, J. P.; Dougherty, D. A. Cation-π Interactions in Structural Biology. *Proc. Natl. Acad. Sci.* **1999**, *96*, 9459–9464, DOI: 10.1073/pnas.96.17.9459.

(49) Crowley, P. B.; Golovin, A. Cation-π Interactions in Protein-Protein Interfaces. *Proteins Struct. Funct. Bioinforma.* **2005**, *59*, 231–239, DOI: 10.1002/prot.20417.

(50) Urry, D. W.; Gowda, D. C.; Parker, T. M.; Luan, C.-H.; Reid, M. C.; Harris, C. M.; Pattanaik, A.; Harris, R. D. Hydrophobicity Scale for Proteins Based on Inverse Temperature Transitions. *Biopolymers* **1992**, *32*, 1243–1250, DOI: 10.1002/bip.360320913.

(51) Li, N. K.; Quiroz, F. G.; Hall, C. K.; Chilkoti, A.; Yingling, Y. G. Molecular Description of the LCST Behavior of an Elastin-Like Polypeptide. *Biomacromolecules* **2014**, *15*, 3522–3530, DOI: 10.1021/bm500658w.

(52) Kurzbach, D.; Hassouneh, W.; McDaniel, J. R.; Jaumann, E. A.; Chilkoti, A.; Hinderberger, D. Hydration Layer Coupling and Cooperativity in Phase Behavior of Stimulus Responsive Peptide Polymers. *J. Am. Chem. Soc.* **2013**, *135*, 11299–11308, DOI: 10.1021/ja4047872.

(53) Elvin, C. M.; Carr, A. G.; Huson, M. G.; Maxwell, J. M.; Pearson, R. D.; Vuocolo, T.; Liyou, N. E.; Wong, D. C. C.; Merritt, D. J.; Dixon, N. E. Synthesis and Properties of Crosslinked Recombinant Pro-Resilin. *Nature* **2005**, *437*, 999–1002, DOI: 10.1038/nature04085.

(54) Lyons, R. E.; Lesieur, E.; Kim, M.; Wong, D. C. C.; Huson, M. G.; Nairn, K. M.; Brownlee, A. G.; Pearson, R. D.; Elvin, C. M. Design and Facile Production of Recombinant Resilin-like Polypeptides: Gene Construction and a Rapid Protein Purification Method. *Protein Eng. Des. Sel.* **2007**, *20*, 25–32, DOI: 10.1093/protein/gzl050.

(55) Dutta, N. K.; Truong, M. Y.; Mayavan, S.; Roy Choudhury, N.; Elvin, C. M.; Kim, M.; Knott, R.; Nairn, K. M.; Hill, A. J. A Genetically Engineered Protein Responsive to Multiple Stimuli. *Angew. Chemie Int. Ed.* **2011**, *50*, 4428–4431, DOI: 10.1002/anie.201007920.

(56) Salvi, A. M.; Moscarelli, P.; Bochicchio, B.; Lanza, G.; Castle, J. E. Combined Effects of Solvation and Aggregation Propensity on the Final Supramolecular Structures Adopted by Hydrophobic, Glycine-Rich, Elastin-like Polypeptides. *Biopolymers* **2013**, *99*, 292–313, DOI: 10.1002/bip.22160.

(57) Ruff, K. M.; Roberts, S.; Chilkoti, A.; Pappu, R. V. Advances in Understanding Stimulus-Responsive Phase Behavior of Intrinsically Disordered Protein Polymers. *J. Mol. Biol.* **2018**, *430*, 4619–4635, DOI: 10.1016/j.jmb.2018.06.031.

(58) Li, L.; Tong, Z.; Jia, X.; Kiick, K. L. Resilin-like Polypeptide Hydrogels Engineered for Versatile Biological Function. *Soft Matter* **2013**, *9*, 665–673, DOI: 10.1039/C2SM26812D.

(59) Li, L.; Teller, S.; Clifton, R. J.; Jia, X.; Kiick, K. L. Tunable Mechanical Stability and Deformation Response of a Resilin-Based Elastomer. *Biomacromolecules* **2011**, *12*, 2302–2310, DOI: 10.1021/bm200373p.

(60) Li, L.; Kiick, K. L. Transient Dynamic Mechanical Properties of Resilin-Based Elastomeric Hydrogels. *Front. Chem.* **2014**, *2*, 1–13, DOI: 10.3389/fchem.2014.00021.

(61) Hess, B.; Kutzner, C.; van der Spoel, D.; Lindahl, E. GROMACS 4: Algorithms for Highly Efficient, Load-Balanced, and Scalable Molecular Simulation. *J. Chem. Theory Comput.* **2008**, *4*, 435–447, DOI: 10.1021/ct700301q.

(62) Bonomi, M.; Parrinello, M. Enhanced Sampling in the Well-Tempered Ensemble. *Phys. Rev. Lett.* **2010**, *104*, 190601, DOI: 10.1103/PhysRevLett.104.190601.

(63) Schuster, B. S.; Dignon, G. L.; Tang, W. S.; Kelley, F. M.; Ranganath, A. K.; Jahnke, C. N.; Simpkins, A. G.; Regy, R. M.; Hammer, D. A.; Good, M. C.; Mittal, J. Identifying Sequence Perturbations to an Intrinsically Disordered Protein That Determine Its Phase-Separation Behavior. *Proc. Natl. Acad. Sci.* **2020**, *117*, 11421–11431, DOI: 10.1073/pnas.2000223117.

(64) Whittaker, J. L.; Dutta, N. K.; Knott, R.; McPhee, G.; Voelcker, N. H.; Elvin, C.; Hill, A.; Choudhury, N. R. Tunable Thermoresponsiveness of Resilin via Coassembly with Rigid Biopolymers. *Langmuir* **2015**, *31*, 8882–8891, DOI: 10.1021/acs.langmuir.5b01014.

(65) Kim, M.; Elvin, C.; Brownlee, A.; Lyons, R. High Yield Expression of Recombinant Pro-Resilin: Lactose-Induced Fermentation in E. Coli and Facile Purification. *Protein Expr. Purif.* **2007**, *52*, 230–236, DOI: 10.1016/j.pep.2006.11.003.

(66) Lyons, R. E.; Elvin, C. M.; Taylor, K.; Lekieffre, N.; Ramshaw, J. A. M. Purification of Recombinant Protein by Cold-Coacervation of Fusion Constructs Incorporating Resilin-Inspired Polypeptides. *Biotechnol. Bioeng.* **2012**, *109*, 2947–2954, DOI: 10.1002/bit.24565.

(67) Ferreira, L. A.; Uversky, V. N.; Zaslavsky, B. Y. Effects of the Hofmeister Series of Sodium Salts on the Solvent Properties of Water. *Phys. Chem. Chem. Phys.* **2017**, *19*, 5254–5261, DOI: 10.1039/c6cp08214a.

(68) Nucci, N. V.; Vanderkooi, J. M. Effects of Salts of the Hofmeister Series on the Hydrogen Bond Network of Water. *J. Mol. Liq.* **2008**, *143*, 160–170, DOI: 10.1016/j.molliq.2008.07.010.

(69) Zhao, C.; Dolmans, L.; Zhu, X. X. Thermoresponsive Behavior of Poly(Acrylic Acid- Co-Acrylonitrile) with a UCST. *Macromolecules* **2019**, *52*, 4441–4446, DOI: 10.1021/acs.macromol.9b00794.

(70) Seuring, J.; Agarwal, S. Polymers with Upper Critical Solution Temperature in Aqueous Solution: Unexpected Properties from Known Building Blocks. *ACS Macro Lett.* **2013**, *2*, 597–600, DOI: 10.1021/mz400227y.

(71) Yoshimitsu, H.; Kanazawa, A.; Kanaoka, S.; Aoshima, S. Well-Defined Polymeric Ionic Liquids with an Upper Critical Solution Temperature in Water. *Macromolecules* **2012**, *45*, 9427–9434, DOI: 10.1021/ma301746u.

(72) Bye, J. W.; Falconer, R. J. Thermal Stability of Lysozyme as a Function of Ion Concentration: A Reappraisal of the Relationship between the Hofmeister Series and Protein Stability. *Protein Sci.* **2013**, *22*, 1563–1570, DOI: 10.1002/pro.2355.

(73) Hildebrand, V.; Laschewsky, A.; Päch, M.; Müller-Buschbaum, P.; Papadakis, C. M. Effect of the Zwitterion Structure on the Thermo-Responsive Behaviour of Poly(Sulfobetaine Methacrylates).

Polym. Chem. **2017**, *8*, 310–322, DOI: 10.1039/c6py01220e.

(74) Qamar, S.; Wang, G.; Randle, S. J.; Ruggeri, F. S.; Varela, J. A.; Lin, J. Q.; Phillips, E. C.; Miyashita, A.; Williams, D.; Ströhl, F.; Meadows, W.; Ferry, R.; Dardov, V. J.; Tartaglia, G. G.; Farrer, L. A.; Kaminski Schierle, G. S.; Kaminski, C. F.; Holt, C. E.; Fraser, P. E.; Schmitt-Ulms, G.; Klenerman, D.; Knowles, T.; Vendruscolo, M.; St George-Hyslop, P. FUS Phase Separation Is Modulated by a Molecular Chaperone and Methylation of Arginine Cation-π Interactions. *Cell* **2018**, *173*, 720-734.e15, DOI: 10.1016/j.cell.2018.03.056.

(75) Loughlin, F. E.; Wilce, J. A. TDP-43 and FUS–Structural Insights into RNA Recognition and Self-Association. *Curr. Opin. Struct. Biol.* **2019**, *59*, 134–142, DOI: 10.1016/j.sbi.2019.07.012.

(76) Dzuricky, M.; Rogers, B. A.; Shahid, A.; Cremer, P. S.; Chilkoti, A. De Novo Engineering of Intracellular Condensates Using Artificial Disordered Proteins. *Nat. Chem.* **2020**, *12*, 814–825, DOI: 10.1038/s41557-020-0511-7.

(77) Minoux, H.; Chipot, C. Cation−π Interactions in Proteins: Can Simple Models Provide an Accurate Description? *J. Am. Chem. Soc.* **1999**, *121*, 10366–10372, DOI: 10.1021/ja990914p.

(78) Lin, Y.-H.; Chan, H. S. Phase Separation and Single-Chain Compactness of Charged Disordered Proteins Are Strongly Correlated. *Biophys. J.* **2017**, *112*, 2043–2046, DOI: 10.1016/j.bpj.2017.04.021.

(79) Murthy, A. C.; Dignon, G. L.; Kan, Y.; Zerze, G. H.; Parekh, S. H.; Mittal, J.; Fawzi, N. L. Molecular Interactions Underlying Liquid−liquid Phase Separation of the FUS Low-Complexity Domain. *Nat. Struct. Mol. Biol.* **2019**, *26*, 637–648, DOI: 10.1038/s41594-019-0250-x.

(80) Lau, H. K.; Li, L.; Jurusik, A. K.; Sabanayagam, C. R.; Kiick, K. L. Aqueous Liquid–Liquid Phase Separation of Resilin-Like Polypeptide/Polyethylene Glycol Solutions for the Formation of Microstructured Hydrogels. *ACS Biomater. Sci. Eng.* **2017**, *3*, 757–766, DOI: 10.1021/acsbiomaterials.6b00076.

(81) Cellesi, F.; Tirelli, N.; Hubbell, J. A. Towards a Fully-Synthetic Substitute of Alginate: Development of a New Process Using Thermal Gelation and Chemical Cross-Linking. *Biomaterials* **2004**, *25*, 5115–5124, DOI: 10.1016/j.biomaterials.2003.12.015.

(82) Bader, R.; Zerbe, O. Peptide/Protein NMR. 1–27, DOI: www.chem.uzh.ch/zerbe/PeptidNMR.pdf.

(83) Mahalakshmi, R.; Sengupta, A.; Raghothama, S.; Shamala, N.; Balaram, P. Tryptophan-Containing Peptide Helices: Interactions Involving the Indole Side Chain*. *J. Pept. Res.* **2005**, *66*, 277–296, DOI: 10.1111/j.1399-3011.2005.00301.x.

(84) Rattan, S.; Li, L.; Lau, H. K.; Crosby, A. J.; Kiick, K. L. Micromechanical Characterization of Soft, Biopolymeric Hydrogels: Stiffness, Resilience, and Failure. *Soft Matter* **2018**, *14*, 3478–3489, DOI: 10.1039/C8SM00501J.

(85) Niskanen, J.; Tenhu, H. How to Manipulate the Upper Critical Solution Temperature (UCST)? *Polym. Chem.* **2017**, *8*, 220–232, DOI: 10.1039/C6PY01612J.

(86) Bierma, J. C.; Roskamp, K. W.; Ledray, A. P.; Kiss, A. J.; Cheng, C.-H. C.; Martin, R. W. Controlling Liquid–Liquid Phase Separation of Cold-Adapted Crystallin Proteins from the Antarctic Toothfish. *J. Mol. Biol.* **2018**, *430*, 5151–5168, DOI: 10.1016/j.jmb.2018.10.023.

(87) McManus, J. J.; Lomakin, A.; Ogun, O.; Pande, A.; Basan, M.; Pande, J.; Benedek, G. B. Altered Phase Diagram Due to a Single Point Mutation in Human D-Crystallin. *Proc. Natl. Acad. Sci.* **2007**, *104*, 16856–16861, DOI: 10.1073/pnas.0707412104.

(88) Ray, S.; Maji, S. K. Predictable Phase-Separated Proteins. *Nat. Chem.* **2020**, *12*, 787–789, DOI: 10.1038/s41557-020-0532-2.

(89) Thorson, T. J.; Botvinick, E. L.; Mohraz, A. Composite Bijel-Templated Hydrogels for Cell Delivery. *ACS Biomater. Sci. Eng.* **2018**, *4*, 587–594, DOI: 10.1021/acsbiomaterials.7b00809.

(90) Bansil, R. Phase Separation in Polymer Solutions and Gels. *Le J. Phys. IV* **1993**, *03*, C1-225-C1-235, DOI: 10.1051/jp4:1993119.

(91) Tanaka, H. Phase-Separation Kinetics in Dynamically Asymmetric Binary Fluids: Viscoelastic Effects in Polymer Solutions. *Int. J. Thermophys.* **1995**, *16*, 371–380, DOI: 10.1007/BF01441903.

(92) Firoozmand, H.; Murray, B. S.; Dickinson, E. Microstructure and Rheology of Phase-Separated Gels of Gelatin+oxidized Starch. *Food Hydrocoll.* **2009**, *23*, 1081–1088, DOI: 10.1016/j.foodhyd.2008.07.013.

(93) Zhang, W. Phase Behavior and Phase Separation Kinetics in Polymer Solutions under High Pressure Phase Behavior and Phase Separation Kinetics in Polymer Solutions under High Pressure, Virginia Polytechnic Institute and State University, 2005.

(94) Läuger, J.; Lay, R.; Gronski, W. The Percolation-to-cluster Transition during Spinodal Decomposition of an Off-critical Polymer Mixture. Observation by Light Scattering and Optical Microscopy. *J. Chem. Phys.* **1994**, *101*, 7181–7184, DOI: 10.1063/1.468304.

(95) Takeno, H.; Iwata, M.; Takenaka, M.; Hashimoto, T. Combined Light Scattering and Laser Scanning Confocal Microscopy Studies of a Polymer Mixture Involving a Percolation-to-Cluster Transition. *Macromolecules* **2000**, *33*, 9657–9665, DOI: 10.1021/ma001316u.

(96) Vermonden, T.; Besseling, N. A. M.; van Steenbergen, M. J.; Hennink, W. E. Rheological Studies of Thermosensitive Triblock Copolymer Hydrogels. *Langmuir* **2006**, *22*, 10180–10184, DOI: 10.1021/la062224m.

(97) Yamaguchi, N.; Chae, B.-S.; Zhang, L.; Kiick, K. L.; Furst, E. M. Rheological Characterization of Polysaccharide−Poly(Ethylene Glycol) Star Copolymer Hydrogels. *Biomacromolecules* **2005**, *6*, 1931–1940, DOI: 10.1021/bm0500042.

(98) Oyen, M. L. Mechanical Characterisation of Hydrogel Materials. *Int. Mater. Rev.* **2014**, *59*, 44–59, DOI: 10.1179/1743280413Y.0000000022.

(99) Barney, C. W.; Dougan, C. E.; Mcleod, K. R.; Kazemi-moridani, A.; Zheng, Y. Cavitation in Soft Matter. **2020**, *117*, 9157–9165, DOI: 10.1073/pnas.1920168117.

(100) Oyen, M. L. Nanoindentation of Hydrated Materials and Tissues. *Curr. Opin. Solid State Mater. Sci.* **2015**, *19*, 317–323, DOI: 10.1016/j.cossms.2015.03.001.

(101) Hu, Y.; Zhao, X.; Vlassak, J. J.; Suo, Z. Using Indentation to Characterize the Poroelasticity of Gels. *Appl. Phys. Lett.* **2010**, *96*, 121904, DOI: 10.1063/1.3370354.

(102) Jackson, G. W.; James, D. F. The Permeability of Fibrous Porous Media. *Can. J. Chem. Eng.* **1986**, *64*, 364–374, DOI: 10.1002/cjce.5450640302.

(103) Roberts, S.; Harmon, T. S.; Schaal, J. L.; Miao, V.; Li, K. (Jonathan); Hunt, A.; Wen, Y.; Oas, T. G.; Collier, J. H.; Pappu, R. V; Chilkoti, A. Injectable Tissue Integrating Networks from Recombinant Polypeptides with Tunable Order. *Nat. Mater.* **2018**, *17*, 1154–1163, DOI: 10.1038/s41563-018-0182-6.

(104) Roberts, S.; Miao, V.; Costa, S.; Simon, J.; Kelly, G.; Shah, T.; Zauscher, S.; Chilkoti, A. Complex

Microparticle Architectures from Stimuli-Responsive Intrinsically Disordered Proteins. *Nat. Commun.* **2020**, *11*, 1342, DOI: 10.1038/s41467-020-15128-9.

(105) Acosta, S.; Poocza, L.; Quintanilla-Sierra, L.; Rodríguez-Cabello, J. C. Charge Density as a Molecular Modulator of Nanostructuration in Intrinsically Disordered Protein Polymers. *Biomacromolecules* **2020**, acs.biomac.0c00934, DOI: 10.1021/acs.biomac.0c00934.